Available online at www.sciencedirect.com
ScienceDirect
Geochimica et Cosmochimica Acta 75 (2011) 4321–4339
Geochimica et Cosmochimica Acta
www.elsevier.com/locate/gca

The coupled $\delta^{13}C$-radiocarbon systematics of three Late Glacial/early Holocene speleothems; insights into soil and cave processes at climatic transitions

D. Rudzka [a,*], F. McDermott [a], L.M. Baldini [b], D. Fleitmann [c], A. Moreno [d], H. Stoll [e]

[a] UCD School of Geological Sciences, University College Dublin, Belfield, Dublin 4, Ireland
[b] Department of Earth Sciences, University of Durham, Durham DH1 3LE, UK
[c] Institute of Geological Sciences, University of Bern, Bern, Switzerland
[d] Instituto Pirenaico de Ecologia-CSIC, Avda. Montanana 1005, 50059 Zaragoza, Spain
[e] Departamento de Geologia, Universidad de Oviedo, ClArias de Velasco, s/n 33005 Oviedo, Spain

Received 25 January 2011; accepted in revised form 11 May 2011; available online 23 May 2011

Abstract

The coupled $\delta^{13}C$-radiocarbon systematics of three European stalagmites deposited during the Late Glacial and early Holocene were investigated to understand better how the carbon isotope systematics of speleothems respond to climate transitions. The emphasis is on understanding how speleothems may record climate-driven changes in the proportions of biogenic (soil carbon) and limestone bedrock derived carbon. At two of the three sites, the combined $\delta^{13}C$ and ^{14}C data argue against greater inputs of limestone carbon as the sole cause of the observed shift to higher $\delta^{13}C$ during the cold Younger Dryas. In these stalagmites (GAR-01 from La Garma cave, N. Spain and So-1 from Sofular cave, Turkey), the combined changes in $\delta^{13}C$ and initial ^{14}C activities suggest enhanced decomposition of old stored, more recalcitrant, soil carbon at the onset of the warmer early Holocene. Alternative explanations involving gradual temporal changes between open- and closed-system behaviour during the Late Glacial are difficult to reconcile with observed changes in speleothem $\delta^{13}C$ and the growth rates. In contrast, a stalagmite from Pindal cave (N. Spain) indicates an abrupt change in carbon inputs linked to local hydrological and disequilibrium isotope fractionation effects, rather than climate change. For the first time, it is shown that while the initial ^{14}C activities of all three stalagmites broadly follow the contemporaneous atmospheric ^{14}C trends (the Younger Dryas atmospheric ^{14}C anomaly can be clearly discerned), subtle changes in speleothem initial ^{14}C activities are linked to climate-driven changes in soil carbon turnover at a climate transition.

1. INTRODUCTION

Variations in oxygen and carbon isotopes ($\delta^{18}O$ and $\delta^{13}C$) in speleothems are used widely to reconstruct past climates, but understanding the links between climate change and $\delta^{13}C$ variations remains challenging, because several different processes can result in elevated $\delta^{13}C$ values (Hendy, 1971; Bar-Matthews et al., 1996; Baker et al., 1997; Bar-Matthews et al., 1999; McDermott, 2004; Vacco et al., 2005). Despite these complexities, a common observation is that $\delta^{13}C$ in speleothems tends to be higher during cold/dry intervals (Genty et al., 2003; Frisia et al., 2005; Genty et al., 2006). This shift is normally attributed to decreased inputs of isotopically light biogenic carbon from soil and vegetation sources when climatic conditions deteriorate.

In this paper, we investigate in detail the causes of systematic carbon isotope ($\delta^{13}C$) variations in three European speleothems that were deposited during the major climate shifts associated with the last Termination, using a

* Corresponding author.
E-mail address: dominika.rudzka@ucd.ie (D. Rudzka).

0016-7037/$ - see front matter © 2011 Elsevier Ltd. All rights reserved.
doi:10.1016/j.gca.2011.05.022

combined $\delta^{13}C$ – radiocarbon approach. In the three speleothems, systematic shifts to heavier carbon (higher $\delta^{13}C$) during the cold–dry Younger Dryas (YD) interval had been reported previously (Baldini, 2007; Fleitmann et al., 2009; Moreno et al., 2009a). Following the general approach of Genty et al. (2001), $\delta^{13}C$ and ^{14}C data are combined to distinguish between the several possible processes that could be responsible for the observed shift to higher $\delta^{13}C$ during the YD. The overall objectives of the paper are (i) to improve our understanding of carbon isotope systematics in speleothems and (ii) to understand better the possible responses of different soil carbon pools (labile vs. recalcitrant) to first-order climate transitions. The latter is important in the context of ongoing concerns about the possible release to the atmosphere of large quantities of soil-stored carbon during the current anthropogenic warming episode (Knorr et al., 2005; Davidson and Janssens, 2006; Trumbore, 2009).

The main reservoirs, processes and isotope fractionation steps are depicted schematically in Fig. 1. In general, soils are characterised by high pCO_2 levels as a result of active root respiration by living vegetation and microbial decomposition of pre-existing soil organic matter (Fig. 1), and they provide the major source of carbon in speleothems (Genty et al., 2001). Downward percolating waters dissolve soil CO_2, resulting in weak carbonic acid that in turn dissolves bedrock carbonate to form dissolved inorganic carbon (DIC). Soil CO_2 production is linked to temperature and moisture conditions on a range of timescales (Dörr and Münnich, 1986; Davidson, 1994; Bird et al., 1996). Thus, in cold–dry climates, reduced CO_2 production by root respiration and microbial decomposition is expected to result in lower soil pCO_2, and this has been central to previous explanations of higher $\delta^{13}C$ in speleothems during cold–dry intervals, such as the YD (Bar-Matthews et al., 1999; Genty et al., 2003; Frisia et al., 2005; McDermott et al., 2005; Couchoud et al., 2009).

It is also understood that both the $\delta^{13}C$ and the ^{14}C activity of DIC, and therefore of deposited speleothems, can be influenced by the extent to which isotopic equilibration occurs between the (isotopically light) soil gas and the DIC in downward percolating water. Two end-member situations have been recognised (Hendy, 1971). In 'open systems', isotopic equilibrium is maintained between the DIC and the coexisting isotopically light soil CO_2. By contrast, in 'closed systems', equilibrium is not maintained between DIC and soil CO_2, with the result that the $\delta^{13}C$ of the DIC evolves towards the higher $\delta^{13}C$ values and lower ^{14}C activities of the limestone bedrock during the dissolution process (Hendy, 1971). In practice, cave systems are likely to exhibit some intermediate behaviour between these two end-members. The $\delta^{13}C$ of speleothems also reflects the

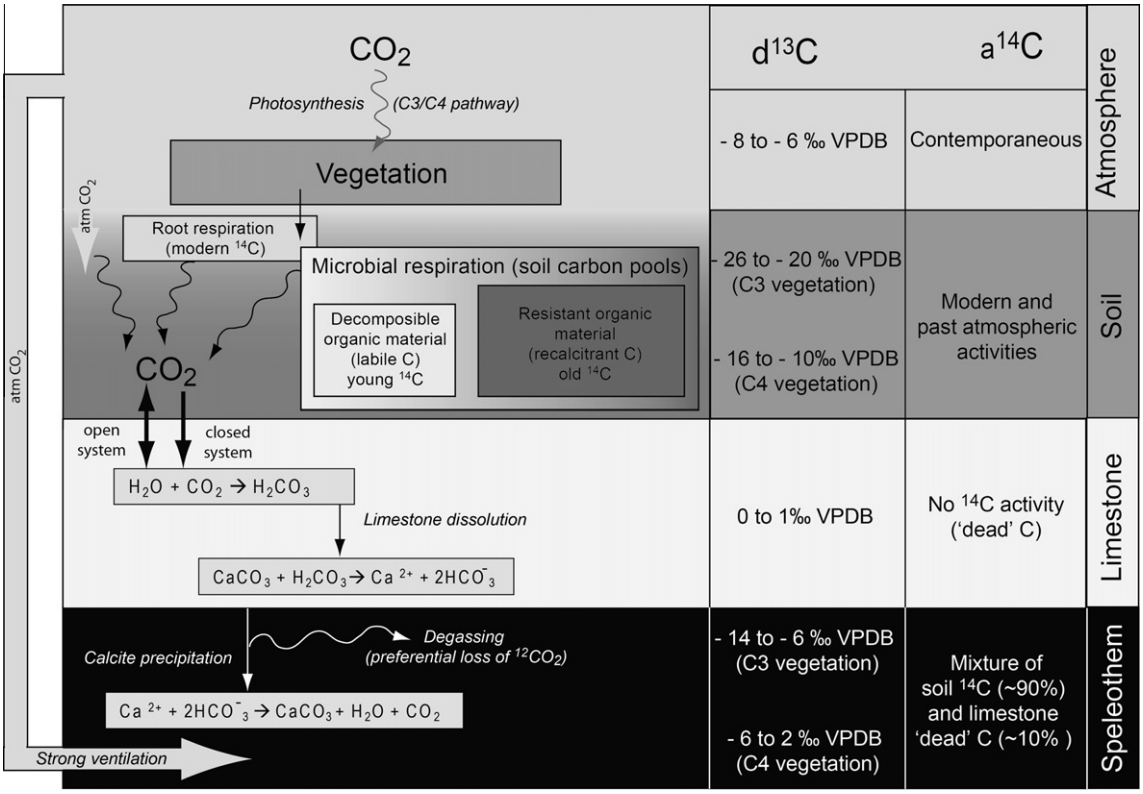

Fig. 1. Schematic diagram of carbon sources in speleothems and their isotopic signatures. The atmosphere has high $\delta^{13}C$ (c. $-6‰$ to $-8‰$ VPDB), and high ^{14}C activity. The $\delta^{13}C$ of the soil gas depends mainly on vegetation type (C3 vs. C4). Both, outward diffusion of soil air CO_2 and admixing of external atmosphere is possible. The ^{14}C activity depends on the mean age of soil carbon, soil respiration processes (microbial vs. live root respiration), and the possible influence of the external atmosphere. Limestone derived carbon typically displays high $\delta^{13}C$ (c. $1‰$ VPDB) and zero radiocarbon activity.

subsequent modification of the $\delta^{13}C$ in DIC by degassing and the isotopic fractionation that accompany carbonate precipitation within caves (Fig. 1).

Disequilibrium isotope fractionation (Mühlinghaus et al., 2009; Scholz et al., 2009) occurs mainly during carbonate precipitation and is promoted by: (i) slower drip rates and (ii) stronger cave ventilation; both of which are more likely in dry–cold conditions. Slower drip rates may increase the speleothem $\delta^{13}C$ values due to the longer time required to re-establish supersaturation with respect to calcite during precipitation between successive drips (Mühlinghaus et al., 2009; Scholz et al., 2009; Dreybrodt and Scholz, 2011). However, rapid degassing, as a consequence of stronger cave ventilation has a relatively small effect on the speleothem $\delta^{13}C$, because it directly affects the $\delta^{13}C$ of dissolved CO_2 only. The speleothem $\delta^{13}C$ by contrast depends mainly on the $\delta^{13}C$ value of the dissolved bicarbonate (more than 95% of DIC), which in turn is influenced largely by calcite precipitation (Dreybrodt and Scholz, 2011). Thus, speleothem $\delta^{13}C$ values may be also affected by the disequilibrium isotope fractionation effect associated with prior calcite precipitation (PCP) which may further increase $\delta^{13}C$ values.

Exceptionally, mixing between the external atmosphere and the cave air can also cause elevated $\delta^{13}C$ and higher ^{14}C activities in strongly ventilated caves (e.g. Spotl et al., 2005; Smith et al., 2009) due to exchange processes of the carbon isotopes between the cave atmosphere and the drip water. However the time constants for this equilibration are long (Dreybrodt and Scholz, 2011) and its importance needs to be investigated further.

The $\delta^{13}C$ of soil CO_2 depends largely on climate driven changes in vegetation type (e.g. C3 vs. C4 plants) and vegetation density. At C3 dominated sites, the $\delta^{13}C$ of soil CO_2 is expected to be in the range $-26‰$ to $-20‰$, whereas C4 vegetation produces soil CO_2 with higher $\delta^{13}C$ ($-16‰$ to $-10‰$) (Wickman, 1952; Hendy, 1971; Salomons and Mook, 1986; Baker et al., 1997; McDermott, 2004). Isotope fractionations between the soil gas, the DIC and precipitated calcite results in $\delta^{13}C$ values in speleothems that are approximately 9.6‰ higher than the soil gas at 12 °C, with only a small temperature dependence (Mook et al., 1974; Mook, 1980). Observed $\delta^{13}C$ values in speleothems deposited at C3 dominated sites are typically in the range $-14‰$ to $-6‰$. Speleothems deposited at C4 dominated sites display correspondingly higher $\delta^{13}C$ values in the range $-6‰$ to $+2‰$ (Fig. 1). However $\delta^{13}C$ in speleothems can extend to higher values than these expected ranges (Baker et al., 1997). A decrease in vegetation density caused by cold–dry climatic conditions can lead to lower CO_2 soil production (and therefore lower soil pCO_2). Low soil pCO_2 can permit stronger downward mixing of atmospheric gases into the soil (Cerling, 1991; Cerling and Quade, 1993; Spotl et al., 2005), resulting in higher $\delta^{13}C$ values in the soil CO_2. Crucially, both the recently fixed labile and stored recalcitrant soil organic pools are biogenic in origin, and their decomposition leads to isotopically light (low $\delta^{13}C$) CO_2. In general these pools cannot be distinguished from each other using $\delta^{13}C$ measurements alone, although there is some evidence that more recalcitrant soil carbon pools of C3 bulk organic matter are characterised by higher $\delta^{13}C$ values compared with the coexisting labile pools (Glaser and Knorr, 2008).

Radiocarbon measurements offer the potential to distinguish between several of these processes and carbon sources. While CO_2 produced by active root respiration reflects the contemporaneous or very recent atmospheric radiocarbon activity (Dörr and Münnich, 1986; Raich and Schlesinger, 1992), respired soil CO_2 is produced by microbial decomposition of pre-existing soil organic matter of variable ages (Hahn et al., 2006). Decomposition of relatively young, recently fixed labile carbon for example, results in a soil CO_2 radiocarbon activity that is close to that of the contemporaneous atmosphere (high ^{14}C activity), whereas old recalcitrant carbon produces soil CO_2 with relatively low ^{14}C activity, reflecting past atmospheric ^{14}C activities that have decayed with time. Progressive dissolution of bedrock carbonate by downward percolating waters dramatically reduces the radiocarbon activity of the DIC, because the ^{14}C activity of limestone-derived carbon is typically zero, and is often referred to as 'dead' carbon (Fig. 1). The observation that speleothem $\delta^{13}C$ tends to be higher during cold/dry intervals (Genty et al., 2003; Frisia et al., 2005; Genty et al., 2006) is usually attributed to decreased inputs of isotopically light root-respired and microbially decomposed (biogenic) carbon.

2. SITE AND SAMPLE DESCRIPTIONS

Stalagmite GAR-01 (Baldini, 2007) was sampled from La Garma cave in Northern Spain (43°25′N, 3°39′W), approximately 13 km ESE of Santander and 6 km inland from the Bay of Biscay (Fig. 2). The cave is developed within La Garma Hill (186 m.a.s.l.) along several sub-horizontal galleries within Early Aptian limestone. The thickness of the overlying bedrock at the sampling site is c. 85 m, and the soil thickness varies from c. 60–150 cm (Baldini, 2007). The top part of La Garma Hill is sparsely vegetated with C3 grasses (Baldini, 2007), whereas the south slope of the hill is densely forested with immature trees (<30 years old) of Bay, Hazel, Eucalyptus and dense undergrowth of ivy and fern. Mean monthly rainfall ranges from a minimum of 52.5 mm in July to a maximum of 159 mm in November (Baldini, 2007), and the mean annual air temperature is c. 13.7 °C (Jackson, 2009).

Sofular cave is located c. 12 km inland from the Black Sea in the Western Pontides (~400 m a.s.l.) near the town of Zonguldak in Northwestern Turkey (41°25′N, 31°56′E) (Fig. 2). This 490 m long cave was formed at a depth of c. 100 m during the Pliocene within Cretaceous limestone (Tuysuz, 1999). The external MAAT is c. 13.81 °C (average for the years 1957–2010; NOAA, 2011), and mean cave air temperature is c. 12 °C. The average precipitation in this region is c. 1200 mm/year, with most of the rainfall falling during September and April. The thickness of the soil above the cave is typically <50 cm. The present-day vegetation above the cave consists mostly of trees, shrubs and C3 grasses (Fankhauser, 2008). Stalagmite So-1 (Fig. 2) is 1.17 m tall and was actively growing when collected in 2006 (Fleitmann et al., 2009).

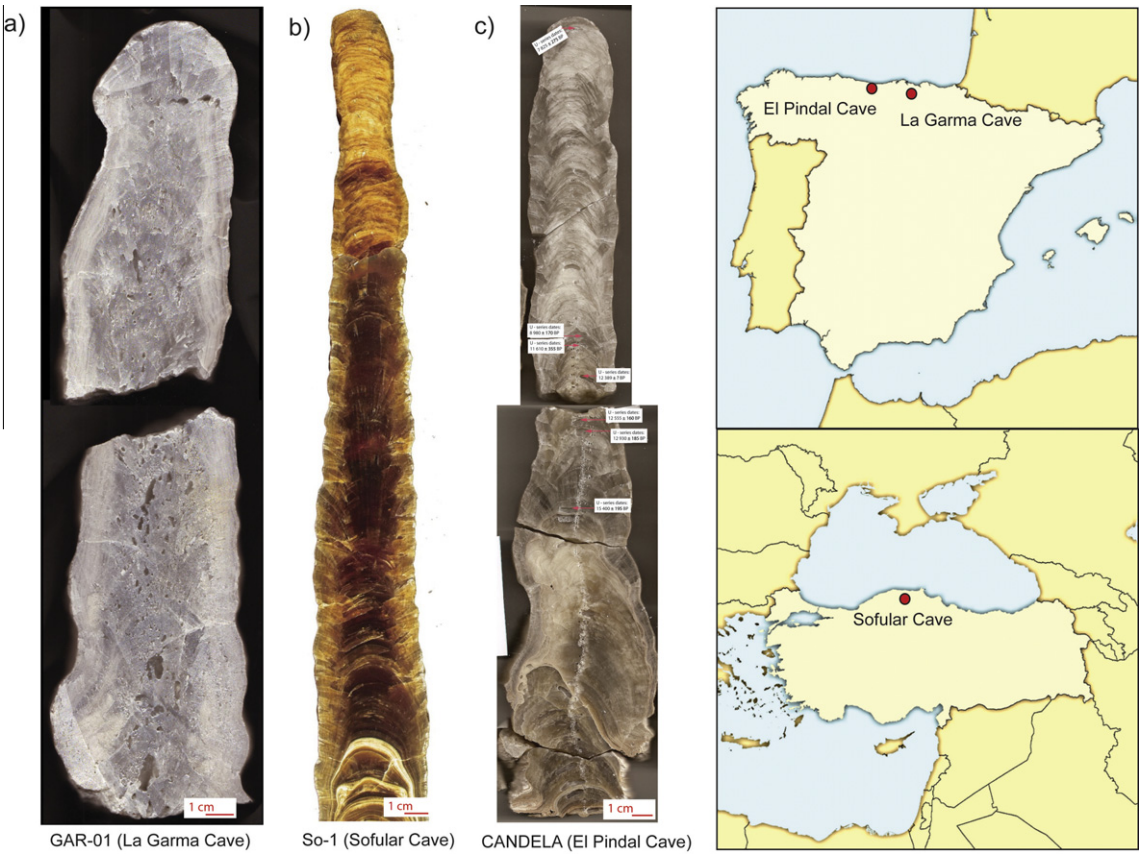

Fig. 2. This figure illustrates the three European stalagmites and the locations of the caves from which they were sampled (Baldini, 2007; Fleitmann et al., 2009; Moreno et al., 2009a).

The Candela stalagmite (Moreno et al., 2009a) was collected from El Pindal Cave in the Asturias region of northern Spain (43°23′N, 4°30′W) (Fig. 2). This 590 m long cave is developed at a depth of 20–60 m in non-dolomitic Carboniferous limestones of the Barcaliente Formation. El Pindal cave is located 24 m.a.s.l., adjacent to the coast. Mean annual rainfall is 1183 ± 175 mm and the mean annual cave temperature is c. 12 °C, similar to the MAAT of the region. The vegetation above the site consists of sparse pasture and gorse shrubs (*Ulex*). The soil cover at this site is relatively thin (0–60 cm). The cave has a large opening and is currently well ventilated, with an average present-day CO_2 concentration of 390 ppm in the cave air (Moreno et al., 2009a). Stalagmite Candela is c. 48.5 cm long, and was collected 500 m from the cave entrance. Candela was growing on a thin (2– 5 cm) crust of flowstone that had collapsed in the past, and as a result this stalagmite could not be linked to a specific drip site. There is evidence for later ceiling collapse that may be related to the opening of new fractures above the Candela drip site and changes in the drip pathways during the YD and Holocene. This increase in drip-rate during the YD is reflected in lower $d^{234}U$ values in the Candela stalagmite (Moreno et al., 2008, 2009a).

All three stalagmites studied here were deposited at sites with an exclusively C3 vegetation (Bottema, 1995; Peñalba et al., 1997; Wick et al., 2003; Moreno et al., 2009b) and were chosen for this study because they contain an unequivocal signal of elevated $\delta^{13}C$ across the YD interval. Published pollen data also indicate clear evidence for climate driven vegetation change, suggesting periglacial conditions during the YD for all three sites (Bottema, 1995; Peñalba et al., 1997; Wick et al., 2003; Moreno et al., 2009b).

3. METHODS

^{14}C activities were measured on 15 sub-samples (10 mg) from stalagmites GAR-01 and So-1, and on fourteen subsamples from Candela stalagmite (Table 1). These new radiocarbon data were coupled with previously reported U-series dates and $\delta^{13}C$ data (Baldini, 2007; Fleitmann et al., 2009; Moreno et al., 2009a). Samples for radiocarbon measurements were drilled using a 1 mm diameter drill bit. Radiocarbon samples from all stalagmites were drilled at the same distance or very close to the previously measured U-series dates. Because of growth-rate variations, each radiocarbon measurement in stalagmite GAR-01 represents 7–18 years during the relatively warm Bølling-Allerød and Holocene, but increases to c. 40 years during the colder YD. In the case of So-1, each measurement averages c. 14 years in the Holocene, c. 20 years in the Bølling-Allerød and YD, and c. 100 years in the Older Dryas. Radiocarbon measurements in Candela represent c. 6.5 years in the Holocene and 30 years during the YD. During the

Table 1
New radiocarbon data combined with previously reported $\delta^{13}C$ data and U-series ages. U-series ages were corrected to 1950 (U/Th dates in bold are from Baldini (2007), Fleitmann et al. (2009), Moreno et al. (2009a). For the Candela stalagmite, distance is calculated from the base, and the sample names in brackets are from Moreno et al. (2008, 2009a). The single $\delta^{13}C$ data point in italics for Candela was previously unpublished. The U/Th dates marked with the asterisk are the interpolated So-1 dates which previously showed an age reversal (shown in brackets). $a^{14}C_m$ is measured radiocarbon activities in each sample. $a^{14}C_{int}$ signifies the initial radiocarbon activity of the sample. $a^{14}C_{atm}$ is the atmospheric radiocarbon activity at the U-series age for each sample and DE is the dilution effect.

Sample name	Distance from top (mm)	Age BP (1950)	Err	^{14}C lab number	Raw ^{14}C age	Err	$a^{14}Cm$	Error (pMC)	$a^{14}C_{int}$	Error (pMC)	$a^{14}C_{atm}$	Error (pMC)	DE (%)	1σ DE_{err}	$\delta^{13}C$
LB 15	796	**13,758**	**120**												
GAR-01 RC1	785	13,571	112	Poz-21523	12,575	57	21.85	0.15	112.80	1.53	119.88	0.86	5.91	1.19	−5.14
GAR-01 RC9	767	13,338	112	Poz-30271	12,140	60	23.03	0.17	115.59	1.57	120.18	0.90	3.82	1.23	−5.81
G1B-2	756	**13,077**	**66**												
GAR-01 RC2	749	13,028	112	Poz-21525	11,961	53	23.53	0.15	113.78	1.54	121.19	0.76	6.13	1.15	−5.45
GAR-01 RC3	725	**12,858**	**115**	Poz-21526	11,585	54	24.62	0.16	116.65	1.62	120.47	0.98	3.18	1.30	−5.66
GAR-01 RC10	718	12,735	112	Poz-30272	11,350	60	25.33	0.18	118.24	1.60	120.28	1.10	1.70	1.35	−4.76
GAR-01 RC4	709	**12,576**	**93**	Poz-21527	11,075	51	26.19	0.16	119.91	1.35	121.99	0.82	1.71	1.08	−4.15
GAR-01 RC11	701	12,263	112	Poz-30273	11,150	60	25.96	0.19	114.41	1.55	120.96	0.29	5.42	0.92	−4.02
GAR-01 RC5	698	12,145	112	Poz-21528	10,802	49	27.07	0.16	117.64	1.59	119.79	0.32	1.80	0.96	−4.47
GAR-01 RC12	690	11,828	112	Poz-30274	10620	50	27.67	0.17	115.73	1.57	118.15	0.31	2.05	0.94	−5.64
GAR-01 RC6	678	**11,353**	**122**	Poz-21529	10,851	49	26.91	0.16	106.26	1.57	114.24	0.26	6.99	0.91	−6.03
GAR-01 RC13	665	11,164	112	Poz-32898	10,390	50	28.45	0.17	109.82	1.49	115.13	0.23	4.62	0.86	−5.78
GAR-01 RC7	646	10,888	112	Poz-21530	10,326	49	28.68	0.17	107.03	1.45	113.18	0.26	5.43	0.85	−6.27
GAR-01 RC14	635	10,728	112	Poz-32899	10,360	50	28.56	0.17	104.55	1.42	112.34	0.27	6.93	0.84	−6.15
GAR-01 RC8	628	**10,626**	**140**	Poz-21531	10318	49	28.70	0.17	103.80	1.76	112.23	0.26	7.52	1.01	−6.03
GAR-01 RC15	601	10,253	112	Poz-32900	10,020	50	29.76	0.18	102.86	1.39	111.40	0.23	7.67	0.81	−6.14
LB9 - GAR01	593	**10,143**	**129**												
So-1 (27)	1223	**17,032**	**178**												
So-1(103C)	1211.12	15,644	108	Poz-30270	14,350	70	17.62	0.15	116.94	1.53	130.52	1.67	10.41	1.60	−7.95
So-1 (10)	1205	**14,929**	**49**												
So-1 (40C)	1203.5	14,814	108	Poz-30269	13,650	60	19.18	0.14	115.12	1.50	126.47	1.38	8.98	1.44	−8.32
So-1 (9)	1202	**14,698**	**36**												
So-1(39C)	1195	**14,585**	**296**	Poz-30268	13,530	70	19.46	0.16	113.61	4.07	123.81	1.06	8.24	2.56	−9.72
So-1 (17C)	1161	**14,295**	**162**	Poz-30267	13,360	70	19.87	0.17	111.97	1.45	120.35	0.91	7.75	1.18	−9.96
		14,034*	108												
So-1(38C)	1150	(13,311)	(102)	Poz-30265	13,300	60	20.01	0.15	109.29	1.42	119.75	0.89	8.98	1.15	−10.24
So-1-(37C)	1124	13,581	108	Poz-30264	12,860	60	21.11	0.15	109.11	1.43	119.94	0.85	9.03	1.14	−10.3
So-1 (8)	1111	**13,355**	**48**												
		13,319*	108												
So-1 (36C)	1108	(12,994)	(126)	Poz-30263	12,640	60	21.67	0.16	108.56	1.42	120.30	0.88	9.76	1.15	−10.35
So-1 (7)	1102	**13,248**	**43**												
So-1 (26C)	1092	**13,091**	**220**	Poz-30262	12,350	60	22.45	0.16	109.38	2.91	120.96	0.82	9.58	1.87	−10.05
So-1 (6)	1083	**12,954**	**48**												
So-1 (a)	1081	**12,921**	**43**												

(*continued on next page*)

Table 1 (*continued*)

Sample name	Distance from top (mm)	Age BP (1950)	Err	^{14}C lab number	Raw ^{14}C age	Err	a^{14}Cm	Error (pMC)	a^{14}C$_{int}$	Error (pMC)	a^{14}C$_{atm}$	Error (pMC)	DE (%)	1σ DE$_{err}$	δ^{13}C
So-1 (4)	1078	**12,794**	**49**												
So-1 (102C)	1080	12,753	108	Poz-30261	11,770	60	24.08	0.17	112.63	1.47	120.24	1.10	6.34	1.29	−8.83
		12,425*	108												
So-1 (35C)	1060	(12,184)	(148)	Poz-30260	11,510	60	24.85	0.18	111.70	1.46	122.33	0.30	8.69	0.88	−8.76
So-1 (3)	1049	**12,200**	**45**												
So-1 (34C)	1044	**11,951**	**150**	Poz-30259	11,390	60	25.21	0.18	107.02	1.94	119.03	0.36	10.10	1.15	-9.31
So-1 (2)	1042	**11,830**	**48**												
So-1 (101C)	1036.8	11,531	108	Poz-30258	11,290	50	25.52	0.15	102.96	1.34	115.74	0.25	11.05	0.80	−10.23
So-1 (1)	1033	**11,313**	**49**												
So-1 (16C)	1024	**11,025**	**156**	Poz-30257	10,910	50	26.72	0.16	101.40	1.91	114.76	024	11.65	1.08	−11.0
So-1 (25C)	999	**10,702**	**104**	Poz-30255	10,500	50	28.08	0.17	102.47	1.29	112.30	0.27	8.75	0.78	−10.44
So-1 (24C)	965	**10,211**	**173**	Poz-30254	10,070	50	29.58	0.18	101.72	2.13	111.65	0.23	8.90	1.18	−10.44
Candela 0 (CAN-B2)	180	**15,394**	**194**	Poz-27434	13370	70	19.84	0.17	127.74	3.00	128.09	1.80	0.27	2.40	−2.92
Candela 15	195	14,237	207	Poz-27435	12,600	70	21.78	0.18	121.89	3.05	120.29	0.93	−1.33	1.99	−6.61
Candela 25 (CAN-1)	205	**13,465**	**200**	Poz-27436	12,130	70	23.05	0.20	117.53	2.84	119.91	0.89	1.99	1.87	−6.95
Candela 35 (CAN-3)	215	**12,838**	**233**	Poz-27438	11,500	60	24.88	0.18	117.53	3.31	120.67	0.98	1.99	1.87	−6.95
Candela 45 (CAN-B3)	225	**12,877**	**186**	Poz-27439	11,470	70	24.97	0.21	118.55	2.67	121.31	0.94	2.27	1.80	−6.98
Candela 47.5	227.5	12,689	207	Poz-32892	11,220	60	25.74	0.19	119.44	2.99	121.61	0.96	1.79	1.97	−5.71
Candela 50 (CAN-C3)	230	**12,500**	**160**	Poz-29253	10,970	60	26.53	0.19	120.33	2.33	121.11	0.58	1.46	1.45	-4.75
Candela 52.5	232.5	12,435	207	Poz-32894	11,020	60	26.37	0.19	118.66	2.97	121.91	0.48	2.67	1.72	−4.72
Candela 55	235	12,369	207	Poz-27440	11,410	80	25.15	0.24	112.30	2.81	121.70	0.36	7.72	1.58	−4.95
Candela -7.5A	240	12,238	207	Poz-27441	11,040	100	26.30	0.32	115.60	2.89	120.73	0.33	4.25	1.61	−5.49
Candela 0A	247.5	12,042	207	Poz-27442	10,920	60	26.69	0.19	114.54	2.87	119.42	0.35	4.09	1.61	−5.69
Candela 10A	257.5	11,780	207	Poz-27443	10,870	60	26.85	0.19	111.64	2.79	117.88	0.31	5.29	1.55	−5.01
Candela 15A	262.5	11,649	207	Poz-27444	10,830	70	26.98	0.23	110.42	2.76	116.72	0.27	5.40	1.52	−4.85
CAN-A7	270	**11,584**	**356**												
CAN-B4	275	**8923**	**173**												
Candela 30.3A	277.8	8872	207	Poz-27445	8620	60	35.25	0.26	103.10	2.58	108.14	0.21	4.66	1.40	−8.15
CA-B5	310	**8663**	**139**												

Bølling-Allerød and the Older Dryas each ^{14}C measurement averages 45 and 70 years, respectively.

The absolute age of samples drilled between the U-series dated points was estimated by linear interpolation (Table 1). The error estimates of the interpolated absolute ages were obtained by averaging the measured errors of the U-series dates. Three U-series dates from stalagmite So-1 which showed an age reversal (Fleitmann et al., 2009) were omitted, and interpolation was applied using the adjacent U-series ages (Table 1). The Candela stalagmite from El Pindal cave exhibits a single age reversal, (sample Candela 45, Table 1), that was also omitted from the age model. One data point Candela 15 (Table 1) shows ^{14}C initial activity higher than that of the contemporaneous atmosphere implying a larger overall uncertainty in the chronology for the Older Dryas and Bølling-Allerød sections of this stalagmite. Most probably, the age of this sample should be c. 200 years younger. In the case of $\delta^{13}C$ measurements, the mean sampling intervals range from 9.4 years in GAR-01, 10.2 years in So-1 and 43 years in the Candela stalagmite.

All radiocarbon measurements were conducted by the Poznan Radiocarbon Laboratory using a 1.5 SDH-Pelletron Model Compact Carbon AMS spectrometer using the Oxalic Acid II (OxII) standard. Sample preparation involves combustion to CO_2 and further graphitisation. Uncertainties reported by the laboratory for each date range from c. 50–100 years, and are derived from control samples of know age (Goslar et al., 2004).

Measured radiocarbon activities ($a^{14}C_m$) were coupled with U-series dates (Table 1) to calculate radiocarbon activities at the time of deposition (initial ^{14}C activity; $a^{14}C_{int}$) using the standard radiocarbon decay equation. Initial radiocarbon activity ($a^{14}C_{int}$) of stalagmite calcite is influenced by a dilution effect (DE) of 'dead' carbon from limestone (DE_{lim}) and aged soil-derived carbon (DE_{soil}). Taken together, these two inputs are referred to as the 'apparent dead carbon proportion' (dcp_{app}), following the terminology of Genty and Massault (1999) and Genty et al. (1999).

$$dcp_{app} = [1 - (a^{14}C_{int}/a^{14}C_{atm})] \times 100\% \quad (1)$$

However, in this paper we distinguish between the different sources of carbon in stalagmites. Thus, the term (DE_{lim}) will be used to refer to the dead carbon proportion derived from limestone ($a^{14}C = 0$), whereas dilution by mixtures of limestone and aged soil carbon will be referred to more generally as the dilution effect (DE).

$$dcp_{app} = DE \quad (2)$$

where, with respect to the DIC

$$DE = DE_{soil} + DE_{lim} - [0.23 \times (\delta^{13}C_{DIC} - \delta^{13}C_{soil\ CO_2})] \quad (3)$$

Following Genty and Massault (1999), dcp_{app} is obtained by the difference between the contemporaneous atmospheric ^{14}C activity ($a^{14}C_{atm}$) and the calculated initial ^{14}C activity at the time of deposition (from U-series ages). In all calculations, atmospheric ^{14}C activity was averaged over the time interval represented by the 2σ error bars on each U-series date, using atmospheric ^{14}C data from the INTCAL 09 dataset (Reimer et al., 2009).

4. RESULTS

Fig. 3 shows the previously published $\delta^{13}C$ records for the three stalagmites (Baldini, 2007; Fleitmann et al., 2009; Moreno et al., 2009a), along with the new radiocarbon results (Table 1). All three stalagmites exhibit elevated $\delta^{13}C$ values during the YD. The most striking feature of the new radiocarbon data is that initial ^{14}C activities show an even more pronounced increase compared with the ^{14}C atmospheric values during the YD interval, and are higher when compared with the warmer Bølling-Allerød and early Holocene (Fig. 3). The initial ^{14}C activity data for all three stalagmites broadly follow, but plot below the contemporaneous INTCAL09 atmosphere curve (Reimer et al., 2009), reflecting the dilution effect (DE) of 'dead' and/or aged soil carbon. Initial ^{14}C activities in So-1 are displaced further below the atmospheric curve than in GAR-01 and Candela (Fig. 3b); however So-1 shows a smoother profile than the other two stalagmites.

In detail, stalagmites GAR-01 and So-1 show an increase in $\delta^{13}C$ of c. 2‰ during the YD, while in Candela, $\delta^{13}C$ increases by c. 4‰ (VPDB), (Fig. 3; Baldini, 2007; Fleitmann et al., 2009; Moreno et al., 2009a). In stalagmite GAR-01 the earliest part of the record begins in the middle Bølling-Allerød period, but the data for So-1 and Candela extend back to the Older Dryas (Fig. 3). In the early Holocene $\delta^{13}C$ is relatively low, with an average value of −6.02‰ VPDB ($2\sigma = 1.05$, $n = 175$). During the Younger Dryas the average $\delta^{13}C$ is −4.64‰ VPDB ($2\sigma = 1.78$, $n = 85$) and during the Bølling-Allerød the average $\delta^{13}C$ is −5.47‰ VPDB ($2\sigma = 0.94$, $n = 132$). Overall, $\delta^{13}C$ in GAR-01 is close to the upper limit expected at a C3 vegetated site (Baker et al., 1997). Importantly, the radiocarbon data for GAR-01 exhibit a decrease of about 3% in DE values during the transition from the warm Bølling-Allerød to the cold YD, followed by an increase in DE of almost 5% during the transition to the warm early Holocene (Table 1). The mean DE values in GAR-01 for the entire time series is $4.73 \pm 1.03\%$ (1σ). The mean values for the Bølling-Allerød, YD and the early Holocene are $4.76 \pm 1.19\%$, $2.54 \pm 1.09\%$ and $6.53 \pm 0.88\%$, respectively.

In stalagmite So-1 (Fleitmann et al., 2009), the transition from the Older Dryas to the warmer Bølling-Allerød is marked by a decrease in $\delta^{13}C$, with the mean value of −10.10‰ VPDB ($2\sigma = 0.65$, $n = 242$). The mean $\delta^{13}C$ value recorded during the YD for speleothem So-1 is −8.96‰ VPDB ($2\sigma = 0.87$, $n = 75$) (Fleitmann et al., 2009), and as in GAR-01, there is a tendency for $\delta^{13}C$ values to decrease during the course of the YD (Fig. 3b). The transition from the YD to the warmer early Holocene is accompanied by a further decrease in $\delta^{13}C$, with a mean value of −10.58‰ VPDB ($2\sigma = 0.66$, $n = 465$). The radiocarbon data for stalagmite So-1 exhibit an increase in DE values during the course of the YD, that continues into the early Holocene (Fig. 3b, Table 1). The mean DE value in So-1 for the entire time series is $9.21 \pm 1.28\%$ (1σ). Mean

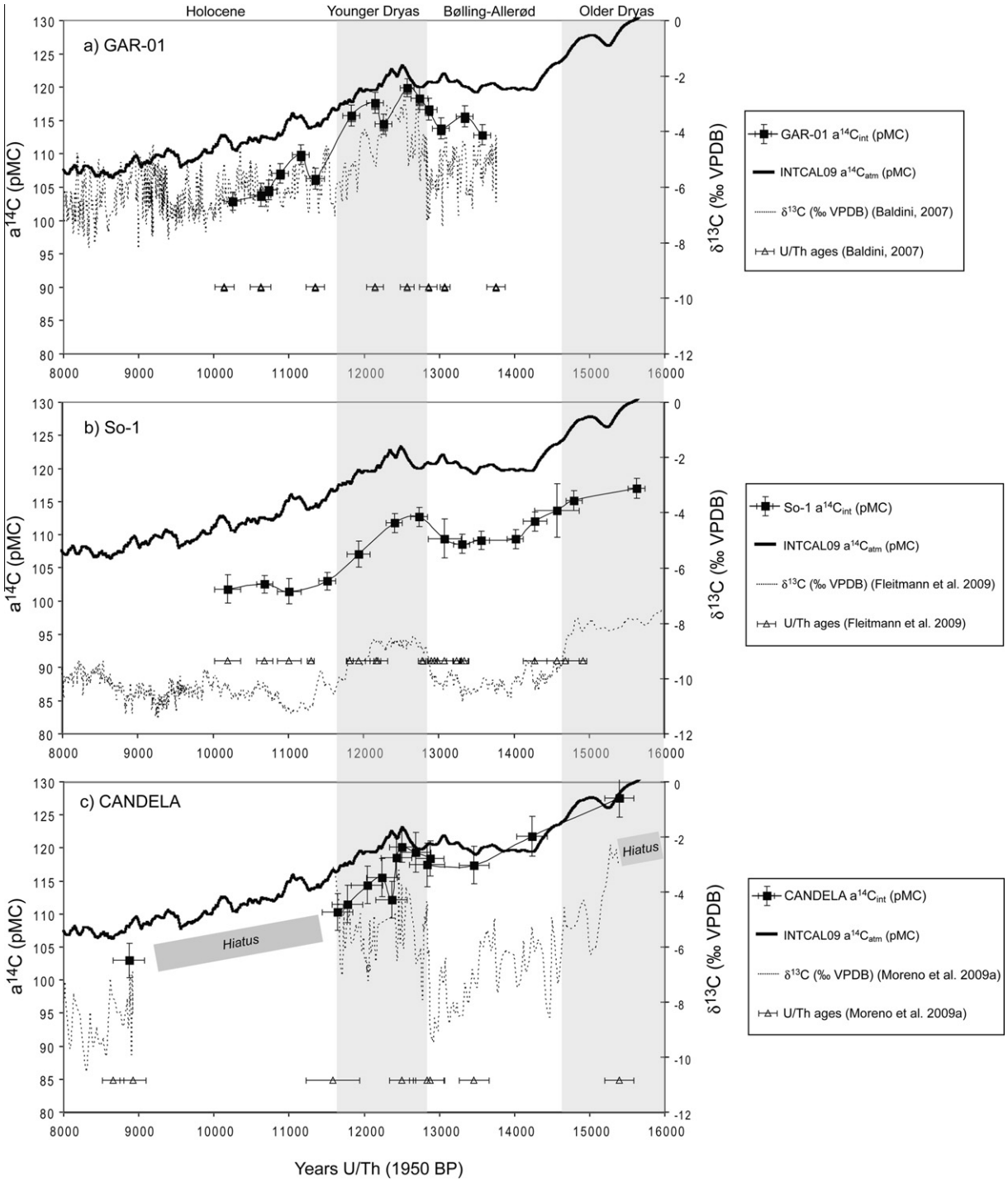

Fig. 3. Plot of initial ^{14}C activities (pMC) and $\delta^{13}C$ data from stalagmites GAR-01 (a), So-1 (b) and Candela (c). Atmospheric ^{14}C activity ($a^{14}C_{atm}$) is plotted as the bold line; using INTCAL 09 (Reimer et al., 2009). Initial ^{14}C activity ($a^{14}C_{int}$) for each stalagmite is plotted with the black solid line; filled squares mark each radiocarbon data point. $\delta^{13}C$ data is plotted with the dashed line and the open triangles represent U-series dates.

values for the Older Dryas, Bølling-Allerød, YD and the early Holocene are $9.69 \pm 1.52\%$, $8.89 \pm 1.51\%$, $8.37 \pm 1.10\%$ and $10.09 \pm 0.96\%$, respectively.

Stalagmite Candela exhibits high $\delta^{13}C$ during the Older Dryas, with a mean value of $-4.49‰$ VPDB ($2\sigma = 2.49$, $n = 19$) (Moreno et al., 2009a). During the warmer Bølling-Allerød period, Candela shows a lower mean $\delta^{13}C$ value of $-7.15‰$ VPDB ($2\sigma = 2.47$, $n = 60$). $\delta^{13}C$ is higher during the YD, with a mean value of $-5.21‰$ VPDB ($2\sigma = 2.15$, $n = 52$). However Candela shows larger

variability in $\delta^{13}C$ than the other two stalagmites; unlike GAR-01 and So-1, there is no long-term trend of decreasing $\delta^{13}C$ during the YD in Candela (Table 1). A hiatus with a duration of c. $2{,}660 \pm 265$ years occurred at the end of the YD. Stalagmite growth recommenced in the early Holocene at $8{,}923 \pm 173$ years BP, and the $\delta^{13}C$ record starting from that date shows a decrease, with the mean value of $-8.43‰$ VPDB ($2\sigma = 1.62$, $n = 44$) (Moreno et al., 2009a). The radiocarbon data for stalagmite Candela imply a DE value of 0.27% for the one data point in the Older Dryas, and a mean value for the Bølling-Allerød of 1.37%. Unlike the other two stalagmites, DE values tend to be higher, not lower, during most of the YD interval (4.08% on average), compared with the Bølling-Allerød, probably reflecting chronological uncertainties in the latter interval. In this stalagmite, the major shift to higher DE values occurs as a step *within* the YD.

Fig. 4 illustrates how the DE values change with time in all three stalagmites. In GAR-01, DE values decrease by c. 3% at the Bølling-Allerød to YD transition, and then increase again by almost 5% at the YD to early Holocene transition (Fig. 4a). Similarly, in So-1, DE values decrease by c. 3% at the Bølling-Allerød to YD transition, and then gradually increase by about 5% through the YD into the early Holocene (curved arrow, Fig. 4b). The lowest DE value is recorded at the beginning of the YD (Fig. 4b). In the Candela stalagmite, DE values are more variable, but there is a marked step-wise change to higher DE values within the YD interval (Fig. 4c). Due to a hiatus after the YD, it is not clear if the DE values continued to increase into the early Holocene as in the other two stalagmites. Also shown on Fig. 4, is the slope of a ^{14}C decay trend that data points would define in a case where a soil carbon reservoir simply gets progressively older, with minimal additional inputs from either limestone derived carbon or recently fixed soil carbon. In general, this in situ ^{14}C decay trend cannot account for the temporal evolution in DE values in any of the stalagmites.

In Fig. 5, the data are presented in plots of $\delta^{13}C$ vs. dilution effect (DE) to investigate the extent to which different carbon sources and processes can be distinguished using combined $\delta^{13}C$ and radiocarbon data. The data for each of the three stalagmites divide into two fields. Also shown on Fig. 5 are the trends that would arise from a number of different processes. Closed system limestone dissolution by downward percolating waters (containing DIC initially in isotopic equilibrium with soil gas), defines sub-horizontal trends on this diagram. The initial soil gas compositions were chosen to represent C3 vegetation derived CO_2 (Closed system curve I), an intermediate/mixed vegetation soil CO_2 (Closed system curve II) and an average C4 vegetation type soil CO_2 respectively (Closed system curve III). These soil gas $\delta^{13}C$ values could also represent different degrees of mixing or isotopic exchange with high $\delta^{13}C$ atmospheric CO_2 (Cerling, 1991). The arrows indicate the evolution of C isotopes during the carbonate dissolution process in a closed system. By contrast, limestone dissolution in a purely open system would result in a steep trend in Fig. 5, because of isotopic re-equilibration with the soil gas, and would be unable to generate a range in DE values. The arrow points in the direction of more complete equilibration between the soil gas and the DIC.

Disequilibrium isotope fractionation (DIF) results in a progressive increase in the $\delta^{13}C$ (sub-vertical arrows on Fig. 5), and this process would be expected to have a greater effect during dry and cold episodes when drip-rates are lower. The $\delta^{13}C$ value of precipitated calcite can increase by c. 3–4‰ as solutions in equilibrium with typical soil CO_2 values degas towards cave atmospheric values (Wiedner et al., 2008; Scholz et al., 2009; Mühlinghaus et al., 2009; Hendy, 1971). In principle the disequilibrium isotope fractionation has a greater effect on $^{14}C/^{12}C$ isotope than on $\delta^{13}C$. However this process has a relatively minor effect on the DE values (which are in percent rather than per mil) resulting in a steep vector on Fig. 5. For every 1‰ increase in $\delta^{13}C$, there is only a 0.2 pMC increase in radiocarbon activity. Therefore, while greater disequilibrium isotope fractionation can explain the large increases in $\delta^{13}C$ during the YD, it cannot in isolation account for large changes (several %) in DE values during and across the YD (Fig. 4 and Fig. 5).

Stalagmite DE values also depend on the age of the decomposing soil carbon that contributes to the soil CO_2 (Fig. 5). Microbial decomposition of relatively young labile soil carbon (higher ^{14}C activity), combined with root respiration, would result in a speleothem high initial radiocarbon activity (low DE value on *x*-axis of Fig. 5). On the other hand, greater inputs of old recalcitrant carbon (lower ^{14}C activity), results in higher speleothem DE values.

In principle, isotopic equilibration between the DIC and the external atmosphere may also play a role and could occur in two ways: (i) by direct mixing of cave air with the external atmosphere in unusually strongly ventilated caves and/or (ii) when depressed soil pCO_2 levels, associated with cold–dry climates facilitate the admixture and exchange with isotopically heavy carbon (pre-industrial $\delta^{13}C$ approximately $-6.5‰$) from the atmosphere (Cerling, 1991) resulting in higher speleothem $\delta^{13}C$ (Fig. 5). This mechanism is consistent with seasonal measurements on soil pCO_2 and soil gas $\delta^{13}C$ which show increased $\delta^{13}C$ values during colder months when soil pCO_2 is lower (Rightmire, 1978; Spotl et al. 2005). In all cases, the $\delta^{13}C$ of bicarbonate-rich waters that have equilibrated with this soil-gas/atmospheric mixture (Rightmire and Hanshaw, 1973; Haas et al., 1983; Cerling 1991) would be approximately 10‰ heavier than the mixed gas (Mook et al., 1974).

DATA MODELLING

5.1. Model parameters

To illustrate the possible effects of different soil carbon residence ages and variable limestone-derived carbon inputs on speleothem initial ^{14}C activity, a three pool soil carbon model was constructed, similar to that employed by Genty and Massault (1999). The model predicts a $^{14}C_{int}$ as a result of incorporation of soil carbon pools with different ages and different amounts of limestone derived dead carbon. The choice of soil carbon residence times was guided by the parameters of the CENTURY model (Parton et al.,

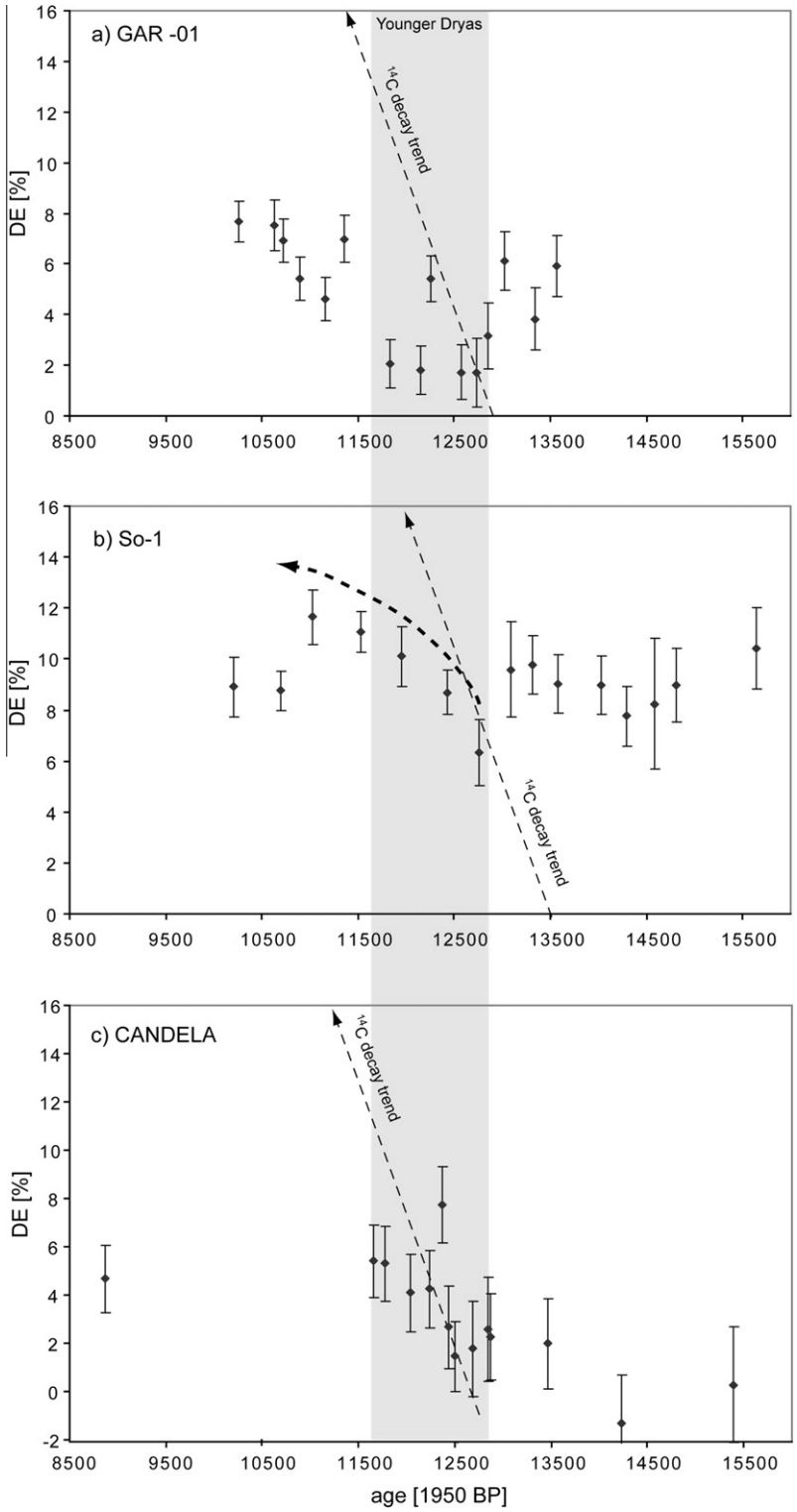

Fig. 4. Plot of dilution effect (DE) against time for stalagmites GAR-01, So-1 and the Candela stalagmite. The data trend that would result from radioactive decay of ^{14}C in a soil is shown for reference on each panel. The curved arrow on panel 4b indicates the gradual increase of DE values towards the Holocene for So-1. Plot shows 1-sigma errors bars.

1987) and other soil carbon studies (Townsend et al. 1997; Trumbore, 2000). In the model, pool C1 represents labile carbon with a short residence time of 1 year (Y1), pool C2 represents an intermediate pool with a 50 years residence time (Y2) and C3 represents a recalcitrant carbon pool with a residence time of >1000 years (Y3). The ^{14}C

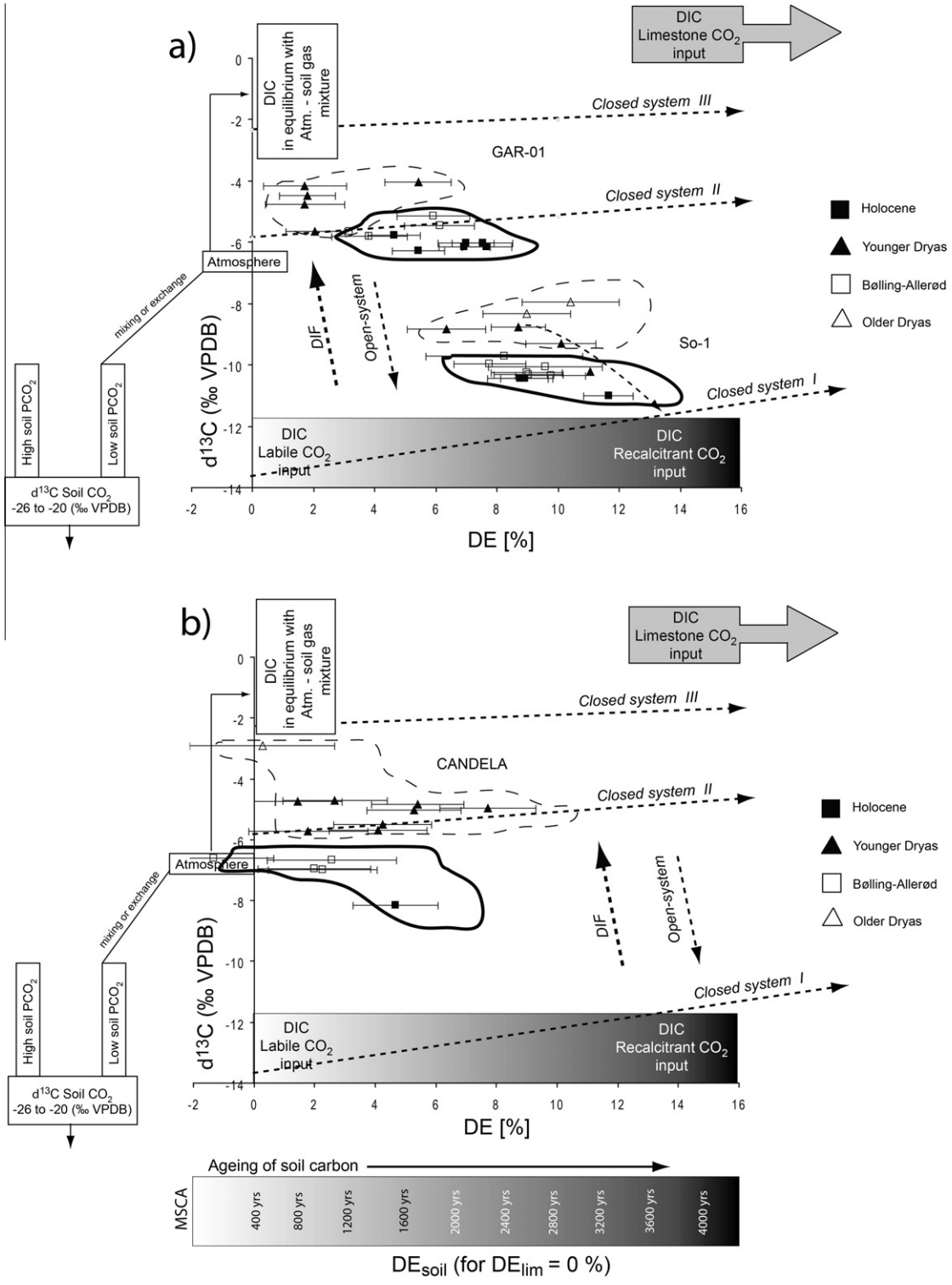

Fig. 5. Plot of speleothem $\delta^{13}C$ against DE values (% dilution of ^{14}C) from three stalagmites in the context of four end-member carbon inputs into the speleothem (limestone, atmosphere, labile and recalcitrant soil carbon pools). Curves (I, II and III) are shown for closed system dissolution with initial soil gas $\delta^{13}C$ values of -23, -15.5 and $-12‰$, respectively, and host-rock limestone with a $\delta^{13}C$ value of 1‰ VPDB. Data points from cold periods (e.g. Older Dryas and YD) are delineated by the dashed line, while the data points for warmer periods (Bølling-Allerød and Holocene) are delineated with the solid bold line. Disequilibrium isotope fractionation results in a steep trend while addition of limestone-derived carbon produces sub-horizontal trends. The x-axis is calibrated to mean soil carbon age (MSCA) values taken from the modelling for the extreme case when $DE_{lim} = 0$ (see Section 5). The curved arrow on panel 5a indicates the gradual increase in DE that is associated with the decrease in $\delta^{13}C$ towards the Holocene for So-1 stalagmite. Plot shows 1-sigma error bars.

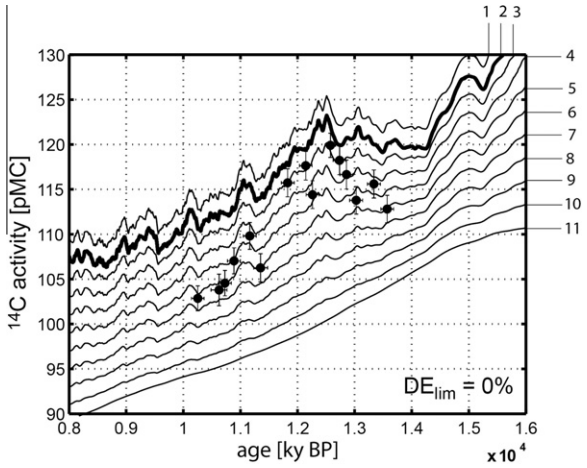

Fig. 6. Plot of model results showing the influence of different soil carbon pools on speleothem DE values. The radiocarbon data from GAR-01 is plotted as a series of data points for the reference. Curve no. 2 is located on the atmospheric ^{14}C activity curve (bold solid curve, Reimer et al. 2009). The influence of soil carbon pools of different ages on stalagmite ^{14}C initial activity is shown by the thin solid curves (from 1 to 11). The dilution effect of limestone (DE_{lim}) was set to zero in order to illustrate how the MSCA influences stalagmite ^{14}C activity. Table 2 shows the MSCA and DE values of each curve. Increasing the proportion of old, recalcitrant carbon soil pool results in a larger dilution effect (DE), which leads to lower stalagmite $^{14}C_{int}$ activities and smoother curves, that plot further from the atmospheric curve.

activity of the atmosphere ($a^{14}C_{atm}$) (Reimer et al. 2009) was corrected using the ^{14}C decay equation for the residence time of each pool and the proportion of carbon pools producing soil CO_2 gas ^{14}C activity ($a^{14}C_g$). This was obtained by mixing three ^{14}C activities from soil pools for each model scenario:

$$a^{14}C_g = C1(a^{14}C_{atm-Y1}) + C2(a^{14}C_{atm-Y2}) + C3(a^{14}C_{atm-Y3}) \text{(Genty and Massault, 1999)} \quad (4)$$

The initial ^{14}C activity of the DIC in equilibrium with the soil gas was calculated taking into account the $^{14}C/^{12}C$ ratio fractionation as a proportion of the $^{13}C/^{12}C$ fractionation (Saliège and Fontes, 1984; Genty and Massault, 1999). The modelled ^{14}C activity in the DIC was also influenced by a limestone derived 'dead' carbon component (DE_{lim}) that could be varied in different model runs. Finally, the ^{14}C activity in speleothem calcite was calculated from equilibrium $^{13}C/^{12}C$ isotope fractionation between bicarbonate and calcite (Genty and Massault, 1999).

5.2. Model results and preliminary interpretations

In the first set of model runs, to explore the potential influence of different soil carbon pools on speleothem DE values, we calculated only the dilution effect of soil carbon (DE_{soil}) on $a^{14}C_{int}$ holding DE_{lim} constant at zero (Fig. 6). The calculated DE_{soil} values include all the main isotope fractionation effects. The purpose of this illustrative model was to explore the maximum mean soil carbon age (MSCA) that the data allow in the limiting case where DE_{lim} is negligible (Fig. 6, Table 2). By mixing soil carbon pools in different proportions (C_i) and residence time (Y_i) different MSCA values can be produced ($MSCA = (C1^{*}Y1 + C2^{*}Y2 + C3^{*}Y3)$), that have an influence on the initial ^{14}C activity curves (Fig. 6). In cases with young MSCA values (atmospheric-like) and $DE_{lim} < 2\%$, the modelled $a^{14}C_{int}$ plots slightly above the atmospheric curve. This arises because the DIC-soil gas fractionation factor for $^{14}C/^{12}C$ in per mil is 2.3 times that for $^{13}C/^{12}C$ (Saliège and Fontes, 1984). Therefore, the minimum DE_{lim} required to ensure that modelled DE values are not negative is 2%. Soil carbon dominated by old pools produces ^{14}C activities with a much greater dilution effect (DE), resulting in a smooth $a^{14}C_{int}$ curve, well below the atmospheric values. The data for GAR-01 are shown on Fig. 6 for reference, and the *maximum* MSCA age that allows to model ^{14}C data at this site is in the order of c. 2400 years.

Pollen records relevant to these sites indicate vegetation changes during the transition periods between Bølling-Allerød – YD and YD – Holocene at all three sites (Moreno et al., 2009b; Peñalba et al., 1997; Bottema, 1995; Wick et al., 2003). The presence of dense and well developed vegetation during the Bølling-Allerød is consistent with high soil organic matter storage capacity and allows the

Table 2
Values of mean soil carbon age (MSCA) and DE_{soil} which were used to construct curves in Fig. 6. The proportion of carbon pools (fast – C1, intermediate – C2 and recalcitrant – C3) along with their residence time (Y1, Y2 and Y3) are also given. The DE_{soil} for each curve was calculated by averaging the DE values every 1000 years from 15,000 to 8000 BP.

Curve no.	MSCA	DE_{soil}						
	(years)	(%)	C1	C2	C3	Y1 (years)	Y2 (years)	Y3 (years)
1	1	−1.91	1	0	0	1	50	4000
2	416	−0.06	0.6	0.3	0.1	1	50	4000
3	816	1.49	0.5	0.3	0.2	1	50	4000
4	1215	3.20	0.4	0.3	0.3	1	50	4000
5	1615	4.84	0.3	0.3	0.4	1	50	4000
6	2015	6.52	0.2	0.3	0.5	1	50	4000
7	2415	8.21	0.1	0.3	0.6	1	50	4000
8	2815	9.89	0	0.3	0.7	1	50	4000
9	3210	11.54	0	0.2	0.8	1	50	4000
10	3605	13.18	0	0.1	0.9	1	50	4000
11	4000	14.86	0	0	1	1	50	4000

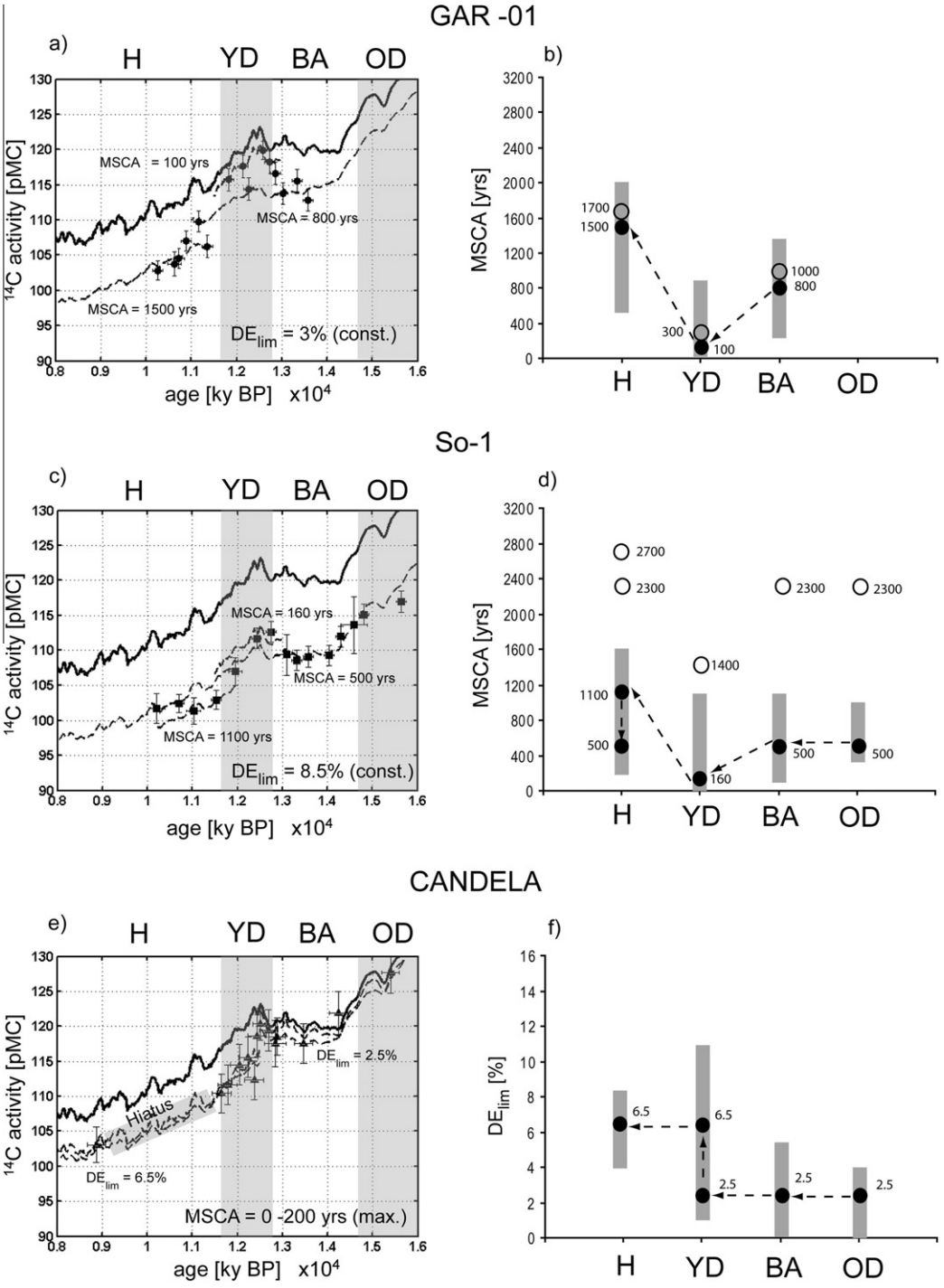

Fig. 7. The initial ^{14}C activity data and model results for stalagmites GAR-01, So-1 and Candela. In the models for GAR-01 and for So-1, the maximum proportion of limestone-derived carbon (DE_{lim}) defined by the YD period, was used and was held constant to assess whether the radiocarbon data for the warmer intervals could be explained by plausible MSCA values. Changes in DE_{lim} by 1% would result in MSCA change by approximately 100 years. The data are modelled by changing the mean soil carbon age (MSCA) during the Late Glacial to Holocene transition (OD – Older Dryas, BA - Bølling-Allerød, YD – Younger Dryas, H – Holocene). By contrast, in model e) for Candela, the MSCA was held constant within a restricted range between 0 and 200 years (marked by two dashed curves), but DE_{lim} changed in the mid-YD from 2.5% to 6.5%. The left hand diagrams (a, c, e) show the best fit of the model to the data. Grey bars on panels b) and d), show the range of MSCA, allowed by the 2-σ error bars of initial ^{14}C activity [pMC] (modelled with 3% and 8.5% DE_{lim} value for GAR-01 and So-1, respectively). Solid symbols indicate the best model fit with 3% DE_{lim} in the panel b) and 8.5% DE_{lim} in the panel d). Open symbols in the panel (b and d) represent the best fit with the *minimum* allowable DE_{lim} value of 2% (model inputs in Table 3 – italics). Grey bars on panel (f) show the range of DE_{lim} and solid symbols represent the best fit of DE_{lim} (modelled with MSCA of 0–200 years) for Candela stalagmite.

possibility for ageing of the soil carbon in the following periods (YD and Holocene). This suggests that the changes in DE values could plausibly be modelled by variable MSCA inputs. Taking the pollen data and the higher inferred biogenic input (lower $\delta^{13}C$ values) during warmer periods into account we constrain modelling assumptions for GAR-01 and So-1. The variable DE values in GAR-1 and So-1 were thus modelled by temporal variations in MSCA values (discussed below). We note that combination of elevated $^{14}C/^{12}C$ ratio (lower DE) and high $\delta^{13}C$ in the cold periods is not readily accounted for by invoking greater limestone inputs. The modelled values of mean soil carbon ages (MSCA) depend on the choice of 'dead' limestone-derived carbon (DE_{lim}) amount. Use of lower DE_{lim} percentages require higher MSCA values to produce a given DE value and vice-versa. However, for simplicity we assumed constant input of limestone-derived carbon (DE_{lim}). The choice of the amount of DE_{lim} was determinated by the maximum amount allowed by the data from the YD period. For example, in the YD section of GAR-01, the maximum value of DE_{lim} is constrained to be c. 3.5% (for the extreme case where the MSCA is set to one year).

Using a constant DE_{lim} value of 3% for GAR-01 (close to the upper limit for the YD), requires an input of much older soil carbon in the Bølling-Allerød (c. 800 years) and Holocene (c. 1500 years) compared with the YD (Fig. 7a, Table 3). Taking the 2σ error bars from this speleothem's $a^{14}C_{int}$ into account, the modelled MSCA shows ranges during each period, presented as a grey band on Fig. 7b. For example, in GAR-01 the MSCA taken from the model output during the Bølling-Allerød ranges from 200 to 1350 years, 1 up to 900 years during the YD, and 500–2000 years during the Holocene (Fig. 7b). Crucially, for GAR-01, the calculated MSCA values are always lower for the YD period compared with the Bølling-Allerød and Holocene, irrespective of the absolute value of DE_{lim} used, assuming that the latter remains relatively constant during the deposition time (Fig. 7b).

Fig. 7c shows the model results for stalagmite So-1. In the YD section of So-1, the maximum value of DE_{lim} is constrained to be c. 9.5% (for the extreme case where the MSCA is set to 1 year). Using a DE_{lim} value of 8.5% (close to this upper limit), requires an input of older soil carbon in the Bølling-Allerød and Holocene compared with the YD. Most of the So-1 data points for the Bølling-Allerød and Older Dryas plot close to a reference curve corresponding to a MSCA value of 500 years (Fig. 7c, Table 3). However, two data points in the early YD require an input of much younger soil carbon age (c. 160 years), and two data points in the early Holocene require older soil carbon input (c. 1100 years) (Fig. 7c, Table 3). The gradual increase in MSCA from the early YD to the early Holocene reflected in a gradual increase in DE (Fig. 4b), suggests greater decomposition of older carbon, stored at the Sofular soil during the YD. Importantly, the modelled MSCA values remain lower for the early YD period compared with the Bølling-Allerød and early Holocene, irrespective of the absolute value of DE_{lim} used (filled and open symbols - Fig. 7d), providing that DE_{lim} remains relatively constant.

The Candela stalagmite data show a wide range in $\delta^{13}C$ (Fig. 5b), much of which can be explained by disequilibrium

Table 3
Model inputs for stalagmites GAR-01, So-1 and Candela for each climatic period of deposition time. The increase in residence time in recalcitrant carbon pool (Y3) in La Garma and Sofular cave sites is implying the ageing of the resistant soil organic matter. Data in italics represents model inputs with the *minimum* DE_{lim} value of 2%, represented as an open symbols on Fig. 7 (panels b and d).

Models	MSCA	DElim						
	(years)	(%)	C1	C2	C3	Y1 (years)	Y2 (years)	Y3 (years)
GAR-01 Bølling-Allerød	800	3	0.210	0.300	0.491	1	50	1600
GAR-01 Younger Dryas	100	3	0.902	0.050	0.048	1	50	2000
GAR-01 Holocene	1500	3	0.302	0.100	0.598	1	50	2500
So-1 Older Dryas	500	8.5	0.243	0.500	0.257	1	50	1850
So-1 Bølling-Allerød	500	8.5	0.243	0.500	0.257	1	50	2000
So-1 Early Younger Dryas	160	8.5	0.830	0.100	0.071	1	50	2200
So-1 Late Younger Dryas	500	8.5	0.243	0.500	0.257	1	50	2200
So-1 Early Holocene	1100	8.5	0.266	0.300	0.434	1	50	2500
So-1 Late Holocene	500	8.5	0.243	0.500	0.257	1	50	2500
CAN Older Dryas	0–200	2.5	0.330	0.300	0.370	1	50	500
CAN Bølling-Allerød	0–200	2.5	0.330	0.300	0.370	1	50	500
CAN Younger Dryas	0–200	6.5	0.330	0.300	0.370	1	50	500
CAN Holocene	0–200	6.5	0.330	0.300	0.370	1	50	500
GAR-01 Bølling-Allerød	*1000*	*2*	*0.084*	*0.300*	*0.616*	*1*	*50*	*1600*
GAR-01 Younger Dryas	*300*	*2*	*0.802*	*0.050*	*0.148*	*1*	*50*	*2000*
GAR-01 Holocene	*1700*	*2*	*0.222*	*0.100*	*0.678*	*1*	*50*	*2500*
So-1 Older Dryas	*2300*	*2*	*0.070*	*0.010*	*0.920*	*1*	*50*	*2500*
So-1 Bølling-Allerød	*2300*	*2*	*0.070*	*0.010*	*0.920*	*1*	*50*	*2500*
So-1 Early Younger Dryas	*1400*	*2*	*0.435*	*0.100*	*0.465*	*1*	*50*	*3000*
So-1 Late Younger Dryas	*2300*	*2*	*0.224*	*0.010*	*0.767*	*1*	*50*	*3000*
So-1 Early Holocene	*2700*	*2*	*0.219*	*0.010*	*0.771*	*1*	*50*	*3500*
So-1 Late Holocene	*2300*	*2*	*0.333*	*0.010*	*0.657*	*1*	*50*	*3500*

isotope fractionation (see Discussion). Unlike in the other two stalagmites, the overall increase in DE values during the Younger Dryas in Candela is not accompanied by a gradual change to lower $\delta^{13}C$ (Fig. 3c). Thus, the YD data for the Candela stalagmite define a sub-horizontal trend on Fig. 5b that could in principle indicate variable DE_{lim} values. Moreover, the absence of a systematic change in DE between the warmer and colder periods in Candela (Fig. 5b, Fig. 7e, Fig. 7f), suggests little or no detectable change in the soil carbon pools undergoing decomposition at this site. The change in DE values during the Younger Dryas can be explained by a relatively small change in DE_{lim} (2.5–6.5%), with the MSCA in the range from 0 to maximum 200 years (Fig. 7e, Fig. 7f). The modelled curve (Fig. 7e) for the later part of the YD fits well to the one data point from the Holocene suggesting that there was no major change in DE_{lim} and/or MSCA during the YD–Holocene transition at this site, although this analysis is hampered by the depositional hiatus in the early Holocene.

6. DISCUSSION

In general, the shifts to higher $\delta^{13}C$ in the colder intervals (relative to the warmer/moister periods) in the Candela stalagmite can be explained to greater closed-system limestone-derived carbon (the YD data plots along a closed-system trend of Fig. 5b), which suggests temporal changes between open-closed system behaviour in this stalagmite. On the other hand, combined changes in $\delta^{13}C$ and DE values in the colder intervals (relative to the warmer/moister periods) in stalagmites GAR-01 and So-1 cannot be attributed solely to greater closed-system limestone-derived carbon (i.e. a shift in the balance between biogenic and limestone-derived carbon), because the data for the colder/drier intervals do not simply plot further to the right along a closed-system limestone dissolution curve on Fig. 5a. Disequilibrium isotope fractionation alone cannot be responsible for this coupled change in $\delta^{13}C$ and DE values, because it has a minimal effect on the latter. Instead, the data for the warmer periods in GAR-01 and So-1 are consistent with: (i) changes in soil respiration balance and atmospheric CO_2 admixture (ii) changes in the response of soil carbon pools to temperature, involving greater decomposition of old, recalcitrant soil carbon during the warmer/moister periods (Bølling-Allerød and Holocene).

6.1. Explanations involving temporal gradations between open and closed system behaviour

As discussed above, variations in DE and $\delta^{13}C$ values in the Candela stalagmite can be explained mainly as a result of changes between open and closed system conditions of limestone dissolution with respect to CO_2 (Fig. 5b) due to site-specific hydrological perturbations. Lower DE values associated with higher $\delta^{13}C$ during the early YD may reflect more open system behaviour when the DIC is in equilibrium with the soil CO_2. The soil at this site is very thin and the vegetation is sparse. Low soil productivity would also permit greater admixing of atmospheric CO_2 into the soil, leading to high ^{14}C activity (low DE) and high $\delta^{13}C$ values. An open, or partly open system would result in greater limestone dissolution compared with a closed system and an increase in the speleothem growth rate. This would arise because increased limestone dissolution, and therefore higher calcium contents in drip waters would give higher growth rates in stalagmites (Baker et al., 1998). During the transition from Bølling-Allerød to YD Candela stalagmite shows increased growth rate (from c. 12 ± 4 to 40 ± 18 μm/year) consistent with our interpretation of more open system conditions.

The increase in DE values in the middle and late YD (associated with relatively high $\delta^{13}C$ values, compared with the Bølling-Allerød or Holocene) could reflect more closed system conditions, where the DIC looses contact with a finite soil gas reservoir and its isotopic signature would no longer reflect soil carbon. This effect is discernable on Fig. 5b, where the YD data for the Candela stalagmite plot along the closed-system trend. Additional variable $\delta^{13}C$ values in Candela can also be explained by changes in disequilibrium isotope fractionation, consistent with trace element ratio arguments presented by Moreno et al. (2009a). Admixture of atmospheric carbon via ventilation (a large cave entrance and low present day CO_2 levels) may also have played a role to some extent. Hydrological changes above the drip site, possibly linked to the collapse of a major ceiling block could account for variable hydrological paths and drip rates and therefore variable disequilibrium isotope fractionation. A faster drip rate and less disequilibrium isotope fractionation during calcite precipitation could explain slightly lower $\delta^{13}C$ values in the middle of YD. In this stalagmite, the step-wise change in DE values during the YD (Fig. 4c) could be caused by variations in open-closed system behaviour and different inputs of limestone-derived carbon (DE_{lim}) due to changes in drip-water hydrology. This latter explanation is underpinned by a marked decrease in initial $\delta^{234}U$ during the YD and Holocene (Moreno et al., 2008, 2009a), which can be linked to enhanced limestone dissolution (e.g. Griffiths et al., 2010; Robinson et al., 2004). Such temporal variations in $\delta^{234}U$ are not observed in the other two stalagmites.

An explanation that involves temporal changes between open-closed system behaviour cannot readily account for higher DE and lower $\delta^{13}C$ values in stalagmites GAR-01 and So-1 during the transition from the YD to the early Holocene. In a closed or partly closed system, higher limestone-derived carbon inputs would increase the DE values due to a greater input of 'dead' carbon which results in higher dilution ^{14}C. However this is not shown in Fig. 5a, where the YD and Holocene data from both stalagmites do not plot along the closed system trend. In both stalagmites, the shift to elevated $\delta^{13}C$ values in the YD tends to be associated with lower DE values. Enhanced disequilibrium isotope fractionation alone cannot account for the magnitude of the shift to lower average DE values, as this process results in a sub-vertical vector in Fig. 5. Similarly, increases in closed-system limestone dissolution leading to higher DE_{lim} during the YD-Holocene transition cannot readily account for the coupled shift in $\delta^{13}C$ and DE, because this process is unable to generate a range in $\delta^{13}C$. During the YD-Holocene transition, the DE in GAR-01

and So-1 changes by about 4‰, and this would produce a shift of c. 0.6‰ towards *heavier* $\delta^{13}C$ values if DE changes were caused solely by greater limestone input in a closed system. However the observed change in $\delta^{13}C$ values at the YD-Holocene transition is c. 2.25‰ towards *lighter* values.

Increased soil pCO_2, in a partly open system would result in greater limestone dissolution and higher stalagmite's growth rates. Stalagmite GAR-01 exhibits increased growth rates during the transition from the YD to the Holocene (from c. 30 ± 2 to c. 70 ± 6 μm/year). Stalagmite So-1 also exhibits higher growth rates during the Holocene compared with the early YD (from c. 25 ± 17 to c. 60 ± 10 μm/year); however the age uncertainties are higher than in GAR-01 due to the presence of an age reversal. However, in a partly open system, the isotopic signature of DIC would reflect soil CO_2 rather the limestone.

Our preferred interpretation at these sites is that GAR-01 and So-1 reflect a partly open system through their entire growth history and that changes in DE values are derived predominantly from changes in the soil carbon inputs.

6.2. Explanation involving variable decomposition rates of soil organic matter

6.2.1. Changes in soil respiration balance and atmospheric admixture

The production of CO_2 in soils is derived from root respiration and microbial decomposition of organic matter (Davidson and Janssens, 2006). During cold and dry climatic conditions (e.g. Younger Dryas), soil CO_2 production rates are expected to decrease due to a lower decomposition rates. That causes a change in the balance between the two sources of soil CO_2, where soil gas is dominated mostly by live root respiration of ambient atmospheric carbon. In addition, overall low soil respiration rates cause lower soil pCO_2 that may in turn allow enhanced downward mixing of atmospheric CO_2 into the soil gas (Cerling, 1991; Spotl et al., 2005). Also reduced vegetation during the YD can result in lower soil pCO_2 that allows greater atmospheric $\delta^{13}C$ admixture into the soil gas. This process can account for the observed low DE and high $\delta^{13}C$ values in GAR-01 and So-1 indicating partly open system behaviour during the YD period. However La Garma site exhibits relatively a thick soil cover. Greater disequilibrium isotope fractionation may therefore play major role in causing the speleothem's higher $\delta^{13}C$ values rather than atmospheric $\delta^{13}C$ admixing into the soil gas.

In the warmer Holocene, CO_2 from decomposition of soil-stored carbon appears to overwhelm CO_2 from root respiration (lower speleothem ^{14}C activity and lower $\delta^{13}C$). Also, higher soil CO_2 productivity reduces admixing of atmospheric CO_2 into the soil gas. Therefore higher DE values (lower ^{14}C activity) during the Holocene in GAR-01 and So-1 can be caused by decomposition of SOM, which overall displays lower ^{14}C activity than CO_2 derived from live root respiration and atmosphere. This explanation does not necessarily involve temperature sensitivity of different soil carbon pools, however it requires higher decomposition rates during warmer climates.

We note that the interpretation involving lower decomposition of soil organic matter and greater root respiration rates during the colder period (YD) is in a contrast to that presented by Dörr and Münnich (1986), where decomposition of SOM occurred mostly during the winter and root respiration during the summer months.

6.2.2. Changes in soil carbon pools temperature sensitivity

Lower DE values (higher ^{14}C activity), coupled with higher $\delta^{13}C$ in GAR-01 during the YD, may reflect reduced decomposition of recalcitrant soil carbon due to the colder/drier conditions. Reduction in the decomposition of old SOM would change the balance towards greater labile carbon inputs (with a more atmospheric-like ^{14}C signature), which could result in lower DE values. Within the YD, the DE values remain low and almost constant. This interpretation implies a different temperature sensitivity of different soil carbon pools and it is supported by the observation that DE values increase progressively during the early Holocene, accompanied by a shift to lower (biogenic) $\delta^{13}C$ (Fig. 5a). This is interpreted to reflect preferential decomposition, following the onset of early Holocene warming, of some of the recalcitrant carbon that was stored during the preceding cold YD episode (Fig. 5a).

The data for the warm and cold periods recorded in stalagmite So-1 similarly do not plot along closed-system limestone input trends in Fig. 5a, indicating that changes in DE_{lim} alone cannot account for the data. Decomposition of older (recalcitrant soil carbon) with lower ^{14}C activities could be responsible for the temporal shift to higher DE values in the late YD and early Holocene in this stalagmite (curved arrow Fig. 4b, Fig. 5a), following a reduction in the decomposition of recalcitrant soil carbon at the onset of the cold/dry YD (as at the La Garma site). Stalagmite So-1 exhibits elevated $\delta^{13}C$ values during the YD, probably due to greater disequilibrium isotope fractionation. In principle, diffusion of atmospheric CO_2 through the thin soil at this site when pCO_2 is reduced could also have played a role and results in elevated $\delta^{13}C$ and ^{14}C. Importantly however, the data points within the YD and the early Holocene intervals, show progressive decreases $\delta^{13}C$ through the late YD and early Holocene (curved arrow, Fig. 5a), which is interpreted as reflecting progressively greater inputs of biogenic soil carbon with time, with no further evidence for increasing atmospheric inputs (high $\delta^{13}C$) during the late YD (Fig. 5a). Thus, DE values in So-1 are low at the beginning of the YD and gradually increase towards the early Holocene (Fig. 4b – curved arrow) reflecting greater input of old SOM. Overall, DE values in So-1 exhibit smooth changes with time suggesting no abrupt changes in hydrologically-driven limestone dissolution rates (unlike Candela). This shift to higher DE values, accompanied by a change to lower $\delta^{13}C$ during the YD–early Holocene transition is interpreted as increased decomposition of stored recalcitrant (^{14}C aged) soil carbon as conditions warm through the late YD into the early Holocene. Importantly, this temporal trend in DE (Fig. 4b) cannot be explained by increases in DE_{lim} alone, because the latter could not produce the observed shift to lower $\delta^{13}C$ (Fig. 5a).

On average, DE values in So-1 are much higher than in the other two stalagmites. Modelling indicates that the overall higher DE values in So-1 cannot be attributed solely to exceptionally old recalcitrant soil carbon, because the required age of this pool would be much too old (c. 10,000 years). Typically, the recalcitrant carbon pools in relatively thin soils (< 1 m) are younger than c. 3000 years, although older fractions can be found in deeper horizons with higher clay and mineral contents (Gaudinski et al., 2000; Trumbore, 2000). In the case of the So-1 data, a significantly older carbon pool would also result in a smoother and displaced (delayed) YD ^{14}C anomaly. The observation, that the temporal trend in ^{14}C initial activity in So-1 broadly follows the shape of the atmospheric ^{14}C curve throughout the Older Dryas to Holocene period (Fig. 3b), suggests that relatively young (c. 500 years) carbon inputs were dominant. Additionally, relatively thin soil cover at Sofular probably provides less opportunity for such long-term (c. 10,000 years) carbon storage. Thus, greater (but relatively constant) inputs of limestone-derived carbon (c. 8.5%) are required compared with the other two stalagmites, but we emphasise that the shifts in DE between the cold and warm periods cannot be explained solely by variable amounts of DE_{lim} for the reasons outlined above.

The combined $\delta^{13}C$ and ^{14}C data (Fig. 5) indicate that the soil gas at Sofular had lower $\delta^{13}C$ values compared with the other two sites. This may reflect the dominance of a more labile carbon pool in the soil, which overall displays slightly lower $\delta^{13}C$ values than recalcitrant pools (Glaser and Knorr, 2008). In general therefore, lower absolute $\delta^{13}C$ values should not necessarily be taken to indicate unusually higher biogenic carbon inputs when comparisons are made between different cave sites.

Overall, the tendency for lower DE values (higher ^{14}C activities) during the cold/dry YD compared with the early Holocene in stalagmites GAR-01 and So-1, can be interpreted as reflecting reduced decomposition rates of the old soil carbon pool.

In principle, the vegetation might also have played a role in increased CO_2 derived from active root respiration, if vegetation type changed from trees to shrubs during the YD. Pollen evidence shows a change from arboreal to non-arboreal pollen during the YD at the La Garma and Sofular sites (Bottema, 1995; Peñalba et al., 1997; Wick et al., 2003; Moreno et al., 2009b). We note that this interpretation (vegetation effect) appears superficially to be consistent with that presented by Dörr and Münnich (1986) for seasonal scale radiocarbon measurements on respired soil CO_2 in the Rhine Valley, near Heidelberg (Germany). In their study, the annual variations in soil gas $^{14}C/^{12}C$ ratio at the grassland site exhibited values closer to atmospheric ^{14}C activities than at a forest site. However their sites did not experience a long-term temporal change in their vegetation as in the sites studied here, which likely affected the $^{14}C/^{12}C$ ratio of the soil carbon. Arboreal vegetation causes higher storage capacity of soil carbon and consequently lower soil ^{14}C activities due to the decomposition of older organic matter. When the vegetation changes from trees to shrubs/grasslands, the older organic matter may still be partially present in the soil due to storage. Therefore such a vegetation change alone at our sites could not in isolation explain higher ^{14}C soil activities during the YD. From this perspective, the study of Dörr and Münnich (1986) involving seasonal variations in soil gas $^{14}C/^{12}C$ ratio from two sites (grassland and forest) may not be applicable to the study of climate induced vegetation changes on the longer timescales studied here. During prolonged cold–dry periods such as the YD for example, it is possible also that higher ^{14}C activities could be enhanced by CO_2 production from root respiration because of root acclimation (Atkin et al., 2000). Arrhenius kinetics argue against the decomposition of recalcitrant soil organic matter during cold intervals such as the YD because it is characterised by higher activation energies (Knorr et al., 2005). From this perspective, decomposition of the more labile soil carbon pools would be the dominant CO_2 source during colder/drier periods, consistent with the shift to lower DE values observed in the YD sections of GAR-01 and So-1.

7. CONCLUSIONS

Increased $\delta^{13}C$ values recorded during the YD in all three stalagmites cannot be accounted for solely by increased inputs of carbon from limestone (i.e. a shift in the balance of biogenic to non-biogenic carbon sources). At the La Garma site, due to a thick soil cover, our preferred explanation is that the combined $\delta^{13}C$ and radiocarbon data reflect climate-driven changes in the soil carbon pools undergoing decomposition, with greater contributions from older soil carbon pools during the warmer/moister periods.

In stalagmite So-1, elevated values of $\delta^{13}C$ and increases in DE values during the YD into the early Holocene can be explained by either a shift in inputs from progressively older soil carbon pools, consistent with the soil carbon temperature sensitivity, as seen in GAR-01. Alternatively, changes in the balance in soil respiration rates and greater atmospheric gas admixture facilitated by a relatively thin soil covercould account for the data. It is also possible that both processes were in operation simultaneously, so that distinguishing between soil carbon pools temperature sensitivity and changes in the soil respiration balance is impossible.

An alternative explanation involving temporal gradations between open and closed system behaviour (Hendy, 1971; Dreybrodt and Scholz, 2011) cannot readily account for the gradual increase in DE values combined with lower $\delta^{13}C$ during the warmer/moister periods in GAR-01 and So-1. Therefore our preferred interpretation of DE changes for these two sites (GAR-01 and So-1) invokes climate-driven changes in soil carbon dynamics, consistent with a greater temperature sensitivity of recalcitrant soil carbon as suggested by Arrhenius kinetics (Knorr et al., 2005).

By contrast, in the Candela stalagmite, the coupled $\delta^{13}C$ and radiocarbon data indicates relatively little change in the mean soil carbon age contributing to the speleothem between the colder and warmer periods, probably as a consequence of the very thin soil cover at this site. An abrupt change in DE values occurs within the YD, but this is attributed to a shift towards greater closed-system limestone-derived carbon inputs (horizontal trends in Fig. 5b), linked to changes in hydrological routing, as reflected in

the initial $\delta^{234}U$ data. The data for Candela can thus be modelled by variable limestone-derived carbon inputs (DE_{lim}), with a restricted range in mean soil carbon ages. The observed signals in Candela stalagmite might not be related to a climate change, but rather to a site specific hydrological effect.

ACKNOWLEDGEMENTS

FMcD and DR gratefully acknowledge financial support from Science Foundation Ireland through the Research Frontiers Programme grant 07/RFP/GEOF265. Authors would like to thank Dr. Denis Scholz, Dr. Jens Fohlmeister and Dr. Miryam Bar-Matthews for their constructive comments and thorough reviews, which improved this manuscript. Also we highly appreciate the efforts of Dr. Miryam Bar-Matthews for her editorial work. DF thankfully acknowledges financial support from the Swiss National Science Foundation (Grant PP002-110554/1). Adelheid Fankhauser is thanked for several discussions about the Sofular site and for sharing the insights gained from her MSc thesis on stalagmite So-1 at the University of Bern.

REFERENCES

Atkin O. K., Edwards E. J. and Loveys B. R. (2000) Response of root respiration to changes in temperature and its relevance to global warming. *New Phyt.* **147**, 141–154.

Baldini, L.M. (2007) *An investigation of the controls on the stable isotope signature of meteoric precipitation, cave seepage water and Holocene stalagmites in Europe*. Ph.D. thesis, University College Dublin.

Baker A., Ito E., Smart P. L. and McEwan R. F. (1997) Elevated and variable values of ^{13}C in speleothems in a British cave system. *Chem. Geol.* **136**(3–4), 263–270.

Baker A., Genty D., Dreybrodt W., Grapes J. and Mockler N. J. (1998) Testing theoretically predicted stalagmite growth rate with recent annually laminated stalagmites: implications for past stalagmite deposition. *Geochim. Cosmochim. Acta* **62**, 393–404.

Bar-Matthews M., Ayalon A., Matthews A., Sass E. and Halicz L. (1996) Carbon and oxygen isotope study of the active water-carbonate system in a karstic Mediterranean cave: implications for paleoclimate research in semiarid regions. *Geochim. Cosmochim. Acta* **60**, 337–347.

Bar-Matthews M., Ayalon A., Kaufman A. and Wasserburg. G. J. (1999) The Eastern Mediterranean paleoclimate as a reflection of regional events: Soreq cave, Israel. *Earth Planet. Sci. Lett.* **166**, 85–95.

Bird M. I., Chivas A. R. and Head J. (1996) A latitudinal gradient in carbon turnover times in forest soils. *Nature* **381**, 143–146.

Bottema, S. (1995) The YD in the eastern Mediterranean. In *Global YD*, vol. 2, *Quat. Sci. Rev.* **14**, 883–891.

Cerling T. E. (1991) Carbon dioxide in the atmosphere: evidence from Mesozoic and Cenozoic paleosols. *Am. J. Sci.* **291**, 377–400.

Cerling T. E. and Quade J. (1993) Stable carbon and oxygen isotopes in soil carbonates. Climate change in continental isotopic records. *Geophys. Monograph* **78**, 217–231.

Couchoud I., Genty D., Hoffmann D., Drysdale R. and Blamart D. (2009) Millennial-scale climate variability during the Last Interglacial recorded in a speleothem from south-western France. *Quat. Sci. Rev.* **28**, 3263–3274.

Davidson, E.A. (1994) Climate change and soil microbial processes: secondary effects are hypothesised from better known interacting primary effects, In *Soil Response to Climate Change* (eds. M.D.A. Rounsevell and P.J. Loveland) NATO ASI Series, Springer-Verlag, Berlin, 23, pp. 156–168.

Davidson E. A. and Janssens I. A. (2006) Temperature sensitivity of soil carbon decomposition and feedbacks to climate change. *Nature* **440**, 165–173.

Dörr H. and Münnich K. O. (1986) Annual variations of the ^{14}C content of soil CO_2. *Radiocarbon* **28**, 338–345.

Dreybrodt W. and Scholz D. (2011) Climatic dependence of stable carbon and oxygen isotope signals recorded in speleothems: from soil water to speleothem calcite. *Geochim. Cosmochim. Acta* **75**, 734–752.

Fankhauser, A. (2008) *Climate variability recorded in 50,000-year old stalagmite from Northern Turkey*. M.Sc. thesis, University of Bern.

Fleitmann D., Cheng H., Badertscher S., Edwards R., Mudelsee M., Göktürk O., Fankhauser A., Pickering R., Raible C. and Matter A. (2009) Timing and climatic impact of Greenland interstadials recorded in stalagmites from northern Turkey. *Geophys. Res. Lett.* **36**, L19707.

Frisia S., Borsato A., Spötl C., Villa I. and Cucchi F. (2005) Climate variability in the SE Alps of Italy over the past 17,000 years reconstructed from a stalagmite record. *Boreas* **34**, 445–455.

Gaudinski J. B., Trumbore S. E., Davidson E. A. and Zheng S. (2000) Soil carbon cycling in a temperate forest: radiocarbon-based estimates of residence times, sequestration rates and partitioning of fluxes. *Biogeochemistry* **51**, 33–69.

Genty D. and Massault M. (1999) Carbon transfer dynamics from bomb-^{14}C and $\delta^{13}C$ time series of a laminated stalagmite from SW France–modelling and comparison with other stalagmite records. *Geochim. Cosmochim. Acta* **63**, 1537–1548.

Genty D., Massault M., Gilmour M., Baker A., Verheyden S. and Kepens E. (1999) Calculation of past dead carbon proportion and variability by the comparison of AMS(14)C and TIMS U/Th ages on two holocene stalagmites. *Radiocarbon* **41**, 251–270.

Genty D., Baker A., Massault M., Proctor C., Gilmour M., Pons-Branchu E. and Hamelin B. (2001) Dead carbon in stalagmites: carbonate bedrock paleodissolution vs. ageing of soil organic matter. Implication for ^{13}C variation in speleothems. *Geochim. Cosmochim. Acta* **65**, 3443–3457.

Genty D., Blamart D., Ouahdi R., Gilmour M., Baker A., Jouzel J. and Van-Exter S. (2003) Precise dating of Dansgaard–Oeschger climate oscillations in western Europe from stalagmite data. *Nature* **421**, 833–837.

Genty D., Blamart D., Ghaleb B., Plagnes V., Causse C., Bakalowicz M., Zouari K., Chkir N., Hellstrom J., Wainer K. and Bourges F. (2006) Timing and dynamics of the last deglaciation from European and North African $\delta^{13}C$ stalagmites profiles – comparison with Chinese and South hemisphere stalagmites. *Quat. Sci. Rev* **25**, 2118–2142.

Glaser B. and Knorr K.-H. (2008) Isotopic evidence for condensed aromatics from non-pyrogenic sources in soils – implications for current methods for quantifying soil black carbon. *Rapid Commun. In Mass Spec.* **22**, 935–942.

Goslar T., Czernik J. and Goslar E. (2004) Low-energy C-14 AMS in Poznan Radiocarbon Laboratory, Poland. *Nucl. Instrum. Methods Phys. Res. B* **223–24**, 5–11.

Griffiths, M.L., Drysdale, R.N., Gagan, M.K., Frisia, S., Zhao, J.-X., Ayliffe, L.K., Hantoro, W.S., Hellstrom, J.C., Fischer, M.J., Feng, Y.-X., Suwargadi, B.W. (2010) Evidence for Holocene changes in Australian – Indonesian monsoon rainfall from stalagmite trace element and stable isotope ratios. *Earth Planet. Sci. Lett.* **292,** 27–38.

Haas H., Fisher D. W., Thorstenson D. C. and Weeks E. P. (1983) $^{13}CO_2$ and $^{14}CO_2$ measurements on soil atmosphere sampled in

the sub-surface unsaturated zone in the western Great Plains of the US. *Radiocarbon* **25**, 301–314.

Hahn V., Högberg P. and Buchmann N. (2006) ^{14}C – a tool for separation of autotrophic and heterotrophic soil respiration. *Global Change Biol.* **12**, 972–982.

Hendy C. H. (1971) The isotopic geochemistry of speleothems I. The calculation of the effects of different modes of formation on the isotopic composition of speleothems and their applicability as paleoclimatic indicators. *Geochim. Cosmochim. Acta* **35**, 801–824.

Jackson, A.S (2009) *Variable sensitivity of European Holocene speleothems to climate change: case studies from selected caves*. Ph.D. thesis, University College Dublin.

Knorr W., Prentice I. C., House J. I. and Holland E. A. (2005) Long-term sensitivity of soil carbon turnover to warming. *Nature* **433**, 298–301.

McDermott F. (2004) Palaeo-climate reconstruction from stable isotope variations in speleothems: a review. *Quat. Sci. Rev.* **23**, 901–918.

McDermott, F., Schwarcz, H., Rowe, P.J. (2005) Isotopes in speleothems, In *Isotopes in Palaeoenvironmental Research* (ed. Leng M.J.) Springer, Netherlands, pp. 185–225.

Mook W. G., Bommerson J. C. and Staverman W. H. (1974) Carbon isotope fractionation between dissolved bicarbonate and gaseous carbon dioxide. *Earth Planet Sci. Lett.* **22**, 169–176.

Mook W. G. (1980) The effect of fossil fuel and biogenic CO, on the ^{13}C and ^{14}C content of atmospheric carbon dioxide. *Radiocarbon* **22**, 392–397.

Moreno, A., Stoll, H., Cacho, I., Vadillo, I., Edwards, R. L., Ito, E., Jiménez-Sánchez, M., Valero-Garcés, B. L. (2008) Paleoclimate reconstruction from the North Iberian Peninsula since last deglaciation: the El Pindal Cave speleothem record (Asturias, Spain), *Geotemas*, **10** (3).

Moreno A., Stoll H., Jimenez-Sanchez M., Cacho I., Valero-Garces B., Ito E. and Edwards R. L. (2009a) A speleothem record of glacial (25–11.6 kyr BP) rapid climatic changes from northern Iberian Peninsula. *Global Planet. Change* **71**, 218–231.

Moreno, A., López-Merino, L., Leira, M., Marco-Barba, J., González-Sampériz, P., Valero-Garcés, B.L., López-Sáez, J.A., Santos, L., Mata, P., Ito, E. (2009b) Revealing the last 13,500 years of environmental history from the multiproxy record of a mountain lake (Lago Enol, northern Iberian Peninsula). *J. Paleolim*., doi:10.1007/s10933-009-9387-7.

Mühlinghaus C., Scholz D. and Mangini A. (2009) Modelling fractionation of stable isotopes in stalagmites. *Geochim. Cosmochim. Acta* **73**, 7275–7289.

NOAA, 2011. National Climate Data Center, Federal Climate Complex, Global Surface Summary of the Day. Version 7, Accessible at http://www7.ncdc.noaa.gov/CDO/dataproduct.

Parton W. J., Schimel D. S., Cole C. V. and Ojima D. S. (1987) Analysis of factors controlling soil organic-matter levels in great-plains grasslands. *Soil Sci. Soc. Am. J.* **51**, 1173–1179.

Peñalba C., Arnold M., Guiot J., Duplessy J.-C. and de Beaulieu J.-L. (1997) Termination of the Last Glaciation in the Iberian Peninsula inferred from the pollen sequence of Quintanar de la Sierra. *Quat. Res.* **48**, 205–214.

Raich J. W. and Schlesinger W. H. (1992) The global carbon dioxide flux in soil respiration and its relationship to vegetation and climate. *Tellus* **44B**, 81–99.

Reimer P. J., Baillie M. G. L., Bard E., Bayliss A., Beck J. W., Blackwell P. G., Bronk Ramsey C., Buck C. E., Burr G. S., Edwards R. L., Friedrich M., Grootes P. M., Guilderson T. P., Hajdas B., Heaton T. J., Hogg A. G., Hughen K. A., Kaiser K. F., Kromer B., McCormac F. G., Manning S. W., Reimer R. W., Richards D. A., Southon J. R., Talamo S., Turney C. S. M., van der Plicht J. and Weyhenmeyer C. E. (2009) IntCal09 and Marine09 radiocarbon age calibration curves, 0–50, 000 yrs cal BP. *Radiocarbon* **51**, 1111–1150.

Rightmire C. T. and Hanshaw B. B. (1973) Relationship between carbon isotope composition of soil CO_2 and dissolved carbonate species in groundwater. *Water Resour. Res.* **9**, 958–967.

Rightmire C. T. (1978) Seasonal variation in pCO_2 and ^{13}C content of soil atmosphere. *Water Resour. Res.* **14**, 691–692.

Robinson L. F., Henderson G. M., Hall L. and Matthews I. (2004) Climatic control of riverine and seawater uranium-isotope ratios. *Science* **305**, 851–854.

Saliège J. F. and Fontes J. C. (1984) Essai de détermination expérimentale du fractionnement des isotopes ^{13}C et ^{14}C du carbone au cours de processus naturels. *Int. J. App. Rad. Iso.* **35**, 55–62.

Salomons, W. and Mook, W.G. (1986) Isotope geochemistry of carbonates in the weathering zone, In *Handbook of Environmental Isotope Geochemistry Vol. 2 The Terrestrial Environment* (eds. P. Fritz and C.J. Fontes), Elsevier, Amsterdam, pp. 239–270.

Scholz D., Mühlinghaus C. and Mangini A. (2009) Modelling the evolution of $\delta^{13}C$ and $\delta^{18}O$ in the solution layer on stalagmite surfaces. *Geochim. Cosmochim. Acta* **73**, 2592–2602.

Smith C. L., Fairchild I. J., Spötl C., Frisia S., Borsato A., Moreton S. G. and Wynn P. M. (2009) Chronology building using objective identification of annual signals in trace element profiles of stalagmites. *Quat. Geochron.* **4**, 11–21.

Spotl C., Fairchild I. J. and Tooth A. F. (2005) Cave air control on dripwater geochemistry, Obir Caves (Austria): implications for speleothem deposition in dynamically ventilated caves. *Geochim. Cosmochim. Acta* **69**, 2451–2468.

Townsend A. R., Vitousek P. M., Desmarais D. J. and Tharpe A. (1997) Soil carbon pool structure and temperature sensitivity inferred using CO_2 and $^{13}CO_2$ incubation fluxes from five Hawaiian soils. *Biogeochemistry* **38**, 1–17.

Trumbore S. (2000) Age of soil organic matter and soil respiration: radiocarbon constraints on belowground C dynamics. *Ecol. Appl.* **10**, 399–411.

Trumbore S. (2009) Radiocarbon and soil carbon dynamics. *Annu. Rev. Earth Planet. Sci.* **37**, 47–66.

Tuysuz O. (1999) Geology of the Cretaceous sedimentary basins of the Western Pontides. *Geol. J.* **34**, 75–93.

Vacco D. A., Clark P. U., Mix A. C., Cheng H. and Edwards R. L. (2005) A speleothem record of YD cooling, Klamath Mountains, Oregon, USA. *Quat. Res.* **64**, 249–256.

Wiedner E., Scholz D., Mangini A., Polag D., Mühlinghaus C. and Segl M. (2008) Investigation of the stable isotope fractionation in speleothems with laboratory experiments. *Quat. Int.* **187**, 15–24.

Wick L., Lemcke G. and Sturm M. (2003) Evidence of Lateglacial and Holocene climatic change and human impact in eastern Anatolia: high-resolution pollen, charcoal, isotopic and geochemical records from the laminated sediments of Lake Van, Turkey. *Holocene* **13**, 665–675.

Wickman F. E. (1952) Variations in the relative abundance of the carbon isotopes in plants. *Geochim. Cosmochim. Acta* **2**, 243–254.

Associate editor: Miryam Bar-Matthews